A generalized Langevin model for turbulent flows

D. C. Haworth and S. B. Pope
School of Mechanical and Aerospace Engineering, Cornell University, Ithaca, New York 14853

(Received 14 January 1985; accepted 24 October 1985)

A Langevin model appropriate to constant property turbulent flows is developed from the general equation for the fluid particle velocity increment proposed by Pope in an earlier paper [Phys. Fluids **26**, 404 (1983)]. This model can be viewed as an analogy between the turbulent velocity of a fluid particle and the velocity of a particle undergoing Brownian motion. It is consistent with Kolmogorov's inertial range scaling, satisfies realizability, and is consistent with second-order closure models. The objective of the present work is to determine the form of a second-order tensor appearing in the general model equation as a function of local mean quantities. While the model is not restricted to homogeneous turbulence, the second-order tensor is evaluated by considering the evolution of the Reynolds stresses in homogeneous flows. A functional form for the tensor is chosen that is linear in the normalized anisotropy tensor and in the mean velocity gradients. The resulting coefficients are evaluated by matching the modeled Reynolds stress evolution to experimental data in homogeneous flows. Constraints are applied to ensure consistency with rapid distortion theory and to satisfy a consistency condition in the limit of two-dimensional turbulence. A set of coefficients is presented for which the model yields good agreement with available data in homogeneous flows.

I. INTRODUCTION

Conventional turbulence modeling[1–3] is based on attempts to close a set of evolution equations for Eulerian mean quantities derived from Eulerian transport equations (e.g., continuity, Navier–Stokes, and scalar transport equations). Alternatively, an evolution equation for the joint probability density function (pdf) of the velocities and scalars can be derived and modeled.[4–6] The latter approach offers several advantages: the joint pdf contains more statistical information than is contained in a finite number of moments and some of the terms that must be modeled in moment closure methods appear in closed form in the pdf evolution equation. The model presented here is a closure of the evolution equation for the Eulerian one-point joint pdf of the velocity field in a constant property turbulent flow.

A Lagrangian viewpoint is useful when modeling, interpreting, and solving pdf evolution equations[7]: the behavior of fluid particles in a turbulent flow provides a complete description of the turbulence. At time t the position and velocity of a fluid particle are denoted by $\hat{\mathbf{x}}(t)$ and $\hat{\mathbf{U}}(t)$. According to the Navier–Stokes equations, in an infinitesimal time interval dt, $\hat{\mathbf{x}}(t)$ and $\hat{\mathbf{U}}(t)$ change by

$$d\hat{x}_i = \hat{U}_i(t)dt\,, \tag{1}$$

and

$$d\hat{U}_i = \left(\nu\nabla^2\langle U_i\rangle - \frac{1}{\rho}\frac{\partial\langle p\rangle}{\partial x_i}\right)dt + \left(\nu\nabla^2 u_i - \frac{1}{\rho}\frac{\partial p'}{\partial x_i}\right)dt\,, \tag{2}$$

where ρ is the density and ν the kinematic viscosity. The Eulerian velocity $\mathbf{U}(\mathbf{x},t)$ and pressure $p(\mathbf{x},t)$ have been decomposed into their means $\langle\mathbf{U}\rangle$ and $\langle p\rangle$ and fluctuations $\mathbf{u}$ and p'. The Eulerian quantities in Eq. (2) are evaluated at the fluid particle location $\mathbf{x} = \hat{\mathbf{x}}(t)$.

We consider the generalized Langevin equation proposed by Pope[8] to model the Lagrangian velocity increment:

$$d\hat{U}_i = \left(\nu\nabla^2\langle U_i\rangle - \frac{1}{\rho}\frac{\partial\langle p\rangle}{\partial x_i}\right)dt + G_{ij}(\hat{U}_j - \langle U_j\rangle)dt + (C_0\epsilon)^{1/2}\,dW_i\,, \tag{3}$$

where $\epsilon(\mathbf{x},t)$ is the dissipation rate of turbulent kinetic energy, $\mathbf{W}(t)$ is an isotropic Weiner process, C_0 is a positive constant, and G_{ij} is a second-order tensor function of local mean quantities. Equation (3) shows that G_{ij} has dimensions of inverse time. This equation is discussed in detail in Sec. II.

The Langevin equation and closely related discrete Markov chains or random walks have been used in studies of turbulent dispersion since Taylor's pioneering paper of 1921.[9] In these Lagrangian calculations, one seeks information on the distribution of passive contaminants embedded in a turbulent flow field; the statistics of the flow field itself (e.g., velocity and length scales) are assumed to be known. The articles by Krasnoff and Peskin,[10] Yaglom,[11] Durbin,[12] and Sawford[13] provide historical insight, theoretical discussion, and extensive bibliographies on the use of Langevin equations in dispersion modeling.

In the present work a Langevin equation is used in a pdf description of turbulence to obtain the Eulerian statistics of the velocity field. This approach was introduced by Chung,[14] who formulated a model based on an analogy between the motion of fluid elements in a turbulent flow and a general Brownian motion. This model was subsequently developed and applied to a variety of flows, including some with chemical reaction, by Chung, Bywater, and Lee.[15–24] Using similar arguments, Langevin equations were used by Kuznetsov and Frost[25,26] both for the fluid particle velocity and for a scalar concentration. Our development (including Ref. 8) differs from the earlier work in two respects. First, the Navier–Stokes equation is retained as the starting point

 0031-9171/86/020387-19$01.90

for the modeling, rather than an analogy between the dynamics of the turbulent flow field and a Brownian motion. This leads to a different physical interpretation of the modeled terms in the Langevin equation. Several constraints on the undetermined coefficients appearing in our model are deduced from the Navier–Stokes equation; results from second-order modeling studies are also used when appropriate (see Sec. IV). The second novel feature of the current work is the anisotropic linear deterministic term in Eq. (3). This allows, in particular, a more satisfactory treatment of the effects of the fluctuating pressure gradient, including the role of the mean velocity gradients (i.e., "rapid" pressure terms).

The purpose of this paper is to present a model for the second-order tensor G_{ij} in terms of the Reynolds stresses $\langle u_k u_l \rangle$, the mean velocity gradients $\partial \langle U_p \rangle / \partial x_q$, and a characteristic turbulent time scale $\tau = \langle u_i u_i \rangle / 2\epsilon$. No scale information can be extracted from this one-point closure, hence τ must be supplied separately.[7] The problem of determining τ is not considered here. When comparing model behavior with experimental data, τ is taken directly from the data as input to the model.

We begin in Sec. II with a discussion of the Langevin equation (Eq. 3) and the rationale for its use in turbulence modeling. It is shown that G_{ij} provides closure for second-order models[1–3] as well as for the pdf evolution equation. In Sec. III we present the general functional form to be developed for G_{ij}, guided by the principles of invariant modeling. Constraints on the resulting model coefficients are then derived in Sec. IV by comparing the modeled Reynolds-stress evolution equations with their exact counterparts derived from the Navier–Stokes equations. The remaining model coefficients are assumed to be constants and are evaluated in Sec. V by matching the modeled evolution of the Reynolds stresses to experimental data in homogeneous turbulent flows. With all model constants determined, we discuss the performance of the model in Sec. VI. It is demonstrated that the model accurately mimics experimental data in virtually every type of homogeneous turbulent flow for which data are available. Finally, in Sec. VII we summarize the results and briefly discuss the extension of the Langevin model to more general classes of turbulent flows.

II. LANGEVIN EQUATION

In this section the physical significance of Eq. (3) and its relevance to turbulence are discussed. It is shown that the Langevin model provides closure for both the pdf evolution equation and for second-order models of turbulence.

By comparing Eqs. (2) and (3) it may be seen that the effects of viscosity and of the fluctuating pressure gradient are modeled by the terms containing G_{ij} and C_0. The final term in Eq. (3) represents a random walk in velocity space: $d\mathbf{W}$ is a joint normal random vector with zero mean and covariance

$$\langle dW_i \, dW_j \rangle = dt \, \delta_{ij} \, . \tag{4}$$

Equation (3) is a linear Markov model for the fluid particle velocity, analogous to the Langevin equation for the velocity of a particle undergoing Brownian motion.[27] In the present context the justification for the stochastic term is that it is consistent with Kolmogorov's (1941) inertial range scaling laws. This is readily seen by forming the Lagrangian structure function

$$\langle \Delta_s \hat{U}_i \Delta_s \hat{U}_j \rangle \equiv \langle [\hat{U}_i(t+s) - \hat{U}_i(t)] [\hat{U}_j(t+s) - \hat{U}_j(t)] \rangle \, . \tag{5}$$

Since G_{ij} is to be modeled as a function of $\langle u_k u_l \rangle$, $\partial \langle U_p \rangle / \partial x_q$, and ϵ, the time scales associated with G_{ij} are the time scale of the mean deformation $T \equiv \| \partial \langle U_p \rangle / \partial x_q \|^{-1}$ and the dissipation time scale τ. For time intervals s such that s is much smaller than T and s is much smaller than τ, Eq. (3) then yields (to first order in s)

$$\langle \Delta_s \hat{U}_i \Delta_s \hat{U}_j \rangle = C_0 \epsilon s \delta_{ij} \, , \tag{6}$$

which agrees with Kolmogorov's (1941) theory[28] and identifies C_0 as a universal constant. This result was first obtained by Obukhov.[29] A value of $C_0 = 2.1$ was determined by Anand and Pope[30] by considering the evolution of the thermal wake behind a line source in grid turbulence.

According to Kolmogorov's (1941) theory, inertial range scaling applies only for time increments s such that $\tau_\eta \ll s \ll \tau$ where τ_η is the Kolmogorov microscale of the turbulence, while Eq. (6) applies for all s much smaller than τ (and s much smaller than T). This shows that the Langevin equation provides a physically realistic model of fluid particle behavior only for $\tau_\eta \ll s \ll \tau$. Equation (3) remains computationally useful for s less than or equal to τ_η, however. Consider N time intervals s_n such that $s_n \leqslant \tau_\eta$, $n = 1,2,\ldots,N$ and $\Sigma_{n=1}^{N} s_n = s$, $\tau_\eta \ll s \ll \tau$. Equation (6) is valid for each s_n and it is readily shown that if we construct $\Delta_s \hat{U}_i' = \Sigma_{n=1}^{N} \Delta_{s_n} \hat{U}_i$, where $\Delta_{s_n} \hat{U}_i = \hat{U}_i(t+s_n) - \hat{U}_i(t)$ by N successive applications of Eq. (3) over the subintervals s_n, then $\langle \Delta_s \hat{U}_i' \rangle = \langle \Delta_s \hat{U}_i \rangle$ and $\langle \Delta_s \hat{U}_i' \Delta_s \hat{U}_j' \rangle = \langle \Delta_s \hat{U}_i \Delta_s \hat{U}_j \rangle$ so that Eq. (6) remains valid for the total time interval s.

There are two assumptions implicit in Eq. (3). First, the Markov property of the model, manifest through the Markov nature of the stochastic process $\mathbf{W}(t)$ and through G_{ij} being a function of local mean quantities, implies that the model applies only to those flows in which all turbulence structure can be expressed in terms of local mean quantities.[31] Second, the isotropic inertial range scaling expressed in Eq. (6) implicitly assumes local isotropy. Flows that are so strongly distorted or have such a low Reynolds number that the small scales are not even approximately isotropic are beyond the scope of this model.

The evolution equation for the Eulerian joint pdf of the velocities $f(\mathbf{V};\mathbf{x},t)$ corresponding to the Navier–Stokes equations is[7]

$$\frac{\partial f}{\partial t} + V_i \frac{\partial f}{\partial x_i} + \left(\nu \nabla^2 \langle U_i \rangle - \frac{1}{\rho} \frac{\partial \langle p \rangle}{\partial x_i} \right) \frac{\partial f}{\partial V_i} = - \frac{\partial}{\partial V_i} [f \langle a_i | \mathbf{V} \rangle] \, , \tag{7}$$

where a_i is the fluctuating component of the fluid particle acceleration

$$a_i \equiv \nu \nabla^2 u_i - \frac{1}{\rho} \frac{\partial p'}{\partial x_i} \, . \tag{8}$$

Since $\langle \mathbf{U} \rangle$ and $\langle p \rangle$ can be expressed in terms of f, the only term in Eq. (7) that needs to be modeled is the conditional expectation of the fluctuating fluid particle acceleration $\langle a_i | \mathbf{V} \rangle$. A corresponding equation is derived from the Langevin model, Eq. (3) (see Ref. 8):

$$\frac{\partial f}{\partial t} + V_i \frac{\partial f}{\partial x_i} + \left(\nu \nabla^2 \langle U_i \rangle - \frac{1}{\rho} \frac{\partial \langle p \rangle}{\partial x_i} \right) \frac{\partial f}{\partial V_i} = -G_{ij} \frac{\partial}{\partial V_i} [f(V_j - \langle U_j \rangle)] + \frac{1}{2} C_0 \epsilon \frac{\partial^2 f}{\partial V_i \, \partial V_i} . \tag{9}$$

Here G_{ij} is a function of local mean quantities and can therefore be expressed in terms of f, and ϵ is assumed to be known. Hence, comparing Eqs. (7) and (9), we see that the Langevin equation provides a closure model for the Eulerian joint pdf equation in which $\langle a_i | \mathbf{V} \rangle$ is modeled as

$$\langle a_i | \mathbf{V} \rangle = G_{ij} (V_j - \langle U_j \rangle) - \frac{1}{2} C_0 \epsilon f^{-1} \frac{\partial f}{\partial V_i} . \tag{10}$$

The Langevin model leads to a valid evolution equation for the pdf $f(\mathbf{V};\mathbf{x},t)$, Eq. (9). Given appropriate initial and boundary conditions for f (i.e., those necessary and sufficient to guarantee a unique solution to the initial and boundary value problem with $f \geq 0$ and $\int \int_{-\infty}^{\infty} \int f \, d\mathbf{V} = 1$ everywhere initially), the Langevin equation with any finite G_{ij} causes f to evolve such that $f \geq 0$ and $\int \int_{-\infty}^{\infty} \int f \, d\mathbf{V} = 1$ for all time. Consequently, f is realizable and all moments deduced from f are realizable; the Langevin model satisfies realizability for any finite G_{ij} (see Ref. 7).

Experiments in homogeneous turbulent flows show that the pdf of the velocity field is a joint normal distribution.[32] Equation (9) admits joint normal solutions in the homogeneous case (G_{ij} and ϵ independent of $\mathbf{x}$). Moreover, for homogeneous turbulence the term containing C_0 in Eq. (9) causes an arbitrary initial pdf to relax to a joint normal distribution. This behavior is a consequence of the term containing G_{ij} in Eq. (3) being linear in $\hat{\mathbf{U}}$, and hence justifies the linear form of the deterministic term in the Langevin equation.

We now investigate the connection between the Langevin equation and second-order closure models. The modeled Reynolds-stress evolution equation is derived from Eq. (9) (see Ref. 8):

$$\frac{\partial \langle u_k u_l \rangle}{\partial t} + \langle U_i \rangle \frac{\partial \langle u_k u_l \rangle}{\partial x_i} + \frac{\partial \langle u_i u_k u_l \rangle}{\partial x_i} + \langle u_i u_k \rangle \frac{\partial \langle U_l \rangle}{\partial x_i} + \langle u_i u_l \rangle \frac{\partial \langle U_k \rangle}{\partial x_i} = G_{ki} \langle u_i u_l \rangle + G_{li} \langle u_i u_k \rangle + C_0 \epsilon \delta_{kl} . \tag{11}$$

The corresponding exact equation is found from the Navier–Stokes equations to be[1–3]

$$\frac{\partial \langle u_k u_l \rangle}{\partial t} + \langle U_i \rangle \frac{\partial \langle u_k u_l \rangle}{\partial x_i} + \frac{\partial \langle u_i u_k u_l \rangle}{\partial x_i} + \langle u_i u_k \rangle \frac{\partial \langle U_l \rangle}{\partial x_i} + \langle u_i u_l \rangle \frac{\partial \langle U_k \rangle}{\partial x_i} = -\frac{1}{\rho} \left\langle u_k \frac{\partial p'}{\partial x_l} \right\rangle - \frac{1}{\rho} \left\langle u_l \frac{\partial p'}{\partial x_k} \right\rangle + \nu \langle u_k \nabla^2 u_l \rangle + \nu \langle u_l \nabla^2 u_k \rangle . \tag{12}$$

In the derivation of moment equations [Eqs. (11) and (12)] from pdf equations [Eqs. (7) and (9)], integrals of a divergence in $\mathbf{V}$ space arise, e.g.,

$$\int \int_{-\infty}^{\infty} \int \frac{\partial}{\partial V_j} [Q(\mathbf{V}) \langle a_j | \mathbf{V} \rangle f(\mathbf{V})] \, d\mathbf{V} .$$

It can be argued both on mathematical and on physical grounds that for a wide class of functions $Q(\mathbf{V})$, including those that appear in the derivation of Eqs. (11) and (12), such integrals are zero.[7] These terms are thus omitted in the Reynolds stress equations.

In second-order modeling, the triple velocity correlation $\langle u_i u_k u_l \rangle$ and all terms on the right-hand side of Eq. (12) need to be modeled. By contrast, no model is needed for the triple velocity correlation term in pdf formulations of the Reynolds-stress equations, such as Eq. (11). This transport term arises from the $V_i \, \partial f / \partial x_i$ term representing convection in physical space in the modeled pdf evolution equation, Eq. (9), and this term is in closed form. Comparing Eqs. (11) and (12), we see that the terms containing G_{ij} and C_0 in Eq. (11) provide closure models for the right-hand side of Eq. (12). Moreover, the tensor G_{ij} can be chosen for compatibility with any second-order closure model that satisfies realizability.

The second-order closure model corresponding to the Langevin equation is found by equating the right-hand sides of Eqs. (11) and (12):

$$G_{ki} \langle u_i u_l \rangle + G_{li} \langle u_i u_k \rangle + C_0 \epsilon \delta_{kl} = -\frac{1}{\rho} \left\langle u_k \frac{\partial p'}{\partial x_l} \right\rangle - \frac{1}{\rho} \left\langle u_l \frac{\partial p'}{\partial x_k} \right\rangle + \nu \langle u_k \nabla^2 u_l \rangle + \nu \langle u_l \nabla^2 u_k \rangle . \tag{13}$$

This compatibility between the Langevin model and second-order models is again a consequence of the linearity of the deterministic term in Eq. (3). In general, second-order closure models do not satisfy realizability without constructing functions of the invariants of $\langle u_k u_l \rangle$ and then imposing constraints to be satisfied in the extreme states.[33] Clearly, the G_{ij} corresponding to a second-order model that violates realizability is not defined when the Reynolds-stress tensor becomes singular. Hence there is an advantage in modeling G_{ij} directly in order to satisfy realizability, then using Eq. (13) to deduce the corresponding Reynolds-stress model.

To summarize, we have shown that the general form of the Langevin model (Eq. 3) is physically justified and that it contains implicit assumptions about the structure of the turbulence. Realizability is satisfied for any finite G_{ij}. The model provides closure for both the pdf evolution equation and for the Reynolds-stress equations.

III. GENERAL MODEL FOR G_{ij}

To complete the model of Eq. (3), it remains to determine the form of the second-order tensor G_{ij} as a function of local mean quantities. The dissipation rate ϵ or time sale τ is assumed known. The modeling proceeds by applying the usual guiding principles of invariant modeling: dimensional consistency, coordinate system independence, Galilean in-

variance, and rules for forming isotropic tensor functions of other tensors.[3,7,33]

We hypothesize that a sufficiently general functional form for G_{ij} is

$$G_{ij} = G_{ij}\left(\langle u_k u_l\rangle, \frac{\partial\langle U_p\rangle}{\partial x_q}, \epsilon\right). \tag{14}$$

Dependence on the mean velocities $\langle U_i\rangle$ is removed by Galilean invariance. We cannot, however, invoke material frame indifference to remove dependence on the antisymmetric components of the mean velocity gradients. The correlations $\langle u_k u_l\rangle$ arise from the convective term in the Navier–Stokes equations and this term does not satisfy material frame indifference.[33] Since G_{ij} appears in the modeled evolution equation for $\langle u_k u_l\rangle$, we do not expect G_{ij} to satisfy material frame indifference either.

The functional form expressed in Eq. (14) can be rigorously justified only in simple situations. In homogeneous flows the velocity pdf is joint normal, hence the mean velocities and the Reynolds stresses provide a complete one-point statistical description of the velocity field. In statistically stationary flows, current values of all Eulerian statistics are equivalent to their past values so that no history of the flow needs to be included in Eq. (14). It is observed experimentally that the large-scale structure of turbulence becomes independent of Reynolds number as the Reynolds number increases, so that no Reynolds number dependence is needed for sufficiently large values of the Reynolds number. It is expected that in more general flows, however, G_{ij} would depend on the velocity field within an integral length scale of a given location $\mathbf{x}$ and on the history of the flow within an integral time scale of the current time t, as well as on a Reynolds number.[31]

No satisfying *a priori* justification can be offered for applying the functional form of Eq. (14) in general flows. However, several observations are made to motivate the use of this simplified form in moderate Reynolds number, nonstationary inhomogeneous turbulence. First, it is observed that some similarity in turbulence structure exists for all Reynolds numbers high enough that the flow is turbulent, although the existence of an inertial subrange and local isotropy in the presence of strong deformation by mean velocity gradients requires a large Reynolds number.[34,35] This provides incentive to try a Reynolds number independent model in situations where the Reynolds number may be too small for a significant inertial subrange to exist, such as wind tunnel experiments. The extension to nonstationary and inhomogeneous flows is more difficult. The ratio of turbulent scales to mean flow scales is typically of order unity in free shear flows and there is no reason to expect that Eq. (14) is an adequate representation under these conditions unless the turbulence is in dynamic equilibrium with the mean flow. Arguments on adopting similar simplified functional forms in the context of moment closures are offered elsewhere (Ref. 3, for example), but justification is provided only *a posteriori* when the performance of the model in a wide range of flows is known. The modeling of inhomogeneous flows using the Langevin equation is deferred to later papers.

A consequence of Eq. (14) is that G_{ij} can be determined by reference to homogeneous flows in which the only relevant velocity field statistics are the mean velocity gradients and the Reynolds stresses. Even with this reduced set of independent variables, the most general functional form of G_{ij} contains more coefficients than can reliably be determined from available experimental data. We instead propose a model for G_{ij} that is linear in the mean velocity gradients and in the Reynolds stresses, or equivalently, that is linear in the mean velocity gradients and in the normalized anisotropy tensor b_{kl}:

$$b_{kl} \equiv \langle u_k u_l\rangle/\langle u_i u_i\rangle - \tfrac{1}{3}\delta_{kl}\,. \tag{15}$$

We then assume (with one exception) that the resulting model coefficients are constants.

The most general form of Eq. (14) that is linear in b_{kl} and in $\partial\langle U_p\rangle/\partial x_q$, and that is consistent with the four principles mentioned at the beginning of this section, is

$$G_{ij} = \alpha_1\frac{1}{\tau}\delta_{ij} + \alpha_2\frac{1}{\tau}b_{ij} + H_{ijkl}\frac{\partial\langle U_k\rangle}{\partial x_l},$$

where

$$\begin{aligned} H_{ijkl} = {} & \beta_1\delta_{ij}\delta_{kl} + \beta_2\delta_{ik}\delta_{jl} + \beta_3\delta_{il}\delta_{jk} \\ & + \gamma_1\delta_{ij}b_{kl} + \gamma_2\delta_{ik}b_{jl} + \gamma_3\delta_{il}b_{jk} \\ & + \gamma_4 b_{ij}\delta_{kl} + \gamma_5 b_{ik}\delta_{jl} + \gamma_6 b_{il}\delta_{jk}\,. \end{aligned} \tag{16}$$

This form includes bilinear terms in b_{kl} and $\partial\langle U_p\rangle/\partial x_q$ ($\gamma_1 - \gamma_6$ terms). Without these there is insufficient flexibility to model experimental data in homogeneous flows.

Equation (11) shows that G_{ij} being linear in $\langle u_k u_l\rangle$ generates terms quadratic in $\langle u_k u_l\rangle$ in the modeled Reynolds-stress equation. Hence the model of Eq. (16) does not correspond to a second-order closure that is linear in the Reynolds stresses.

The most general form of the model for G_{ij} is now reduced to the linear form expressed in Eq. (16). This model is consistent with the principles of invariant modeling and satisfies realizability for any finite values of the model coefficients. We now restrict our attention to homogeneous flows in order to determine the 11 model coefficients.

IV. CONSTRAINTS ON MODEL COEFFICIENTS

Several relationships among the model coefficients are deduced by comparing the modeled Reynolds-stress evolution equation (Eq. 11) to its exact counterpart (Eq. 12) obtained from the Navier–Stokes equations in homogeneous flows. It is found that all 11 of the model coefficients cannot be constants and that the value of one coefficient is indeterminate in constant property flows.

We want to consider the evolution of the Reynolds stresses in statistically homogeneous transient flows. The modeled and the exact Reynolds-stress equations (Eqs. 11 and 12) simplify considerably in this case. Mean velocity gradients can be nonzero but are spatially uniform. Wind tunnel experiments generate statistically stationary turbulence that is homogeneous in the transverse directions but inhomogeneous in the streamwise direction. This approximates the desired homogeneous transient flow field if we consider a coordinate system that moves with the mean flow

velocity: the convective derivative following the mean flow is replaced by a time derivative, $\langle U_i\rangle \partial/\partial x_i \approx d/dt$, and Eqs. (11) and (12) reduce to ordinary differential equations. Conditions under which this approximation is valid are given in Ref. 34. The modeled Reynolds-stress evolution equation simplifies to

$$\frac{d\langle u_k u_l\rangle}{dt} = -\langle u_i u_k\rangle \frac{\partial \langle U_l\rangle}{\partial x_i} - \langle u_i u_l\rangle \frac{\partial \langle U_k\rangle}{\partial x_i} + G_{ki}\langle u_i u_l\rangle + G_{li}\langle u_i u_k\rangle + C_0 \epsilon \delta_{kl}\,, \tag{17}$$

and the exact Reynolds-stress equation becomes

$$\frac{d\langle u_k u_l\rangle}{dt} = -\langle u_i u_k\rangle \frac{\partial \langle U_l\rangle}{\partial x_i} - \langle u_i u_l\rangle \frac{\partial \langle U_k\rangle}{\partial x_i} + \phi_{kl} + \phi_{lk} - \epsilon_{kl}\,, \tag{18}$$

where

$$\phi_{kl} \equiv \frac{1}{\rho}\left\langle p' \frac{\partial u_k}{\partial x_l}\right\rangle, \tag{19}$$

$$\epsilon_{kl} \equiv 2\nu \left\langle \frac{\partial u_k}{\partial x_i}\frac{\partial u_l}{\partial x_i}\right\rangle. \tag{20}$$

Here ϕ_{kl} is the fluctuating pressure-rate-of-strain correlation and ϵ_{kl} is the dissipation tensor.

From an examination of these equations and other considerations, constraints on the model coefficients are now deduced.

A. Evolution of the turbulent kinetic energy

Taking one-half the trace of the Reynolds-stress evolution equation gives an equation for the turbulent kinetic energy $k \equiv \langle u_l u_l\rangle/2$. From Eq. (17) the modeled k equation is

$$\frac{dk}{dt} = -\langle u_k u_l\rangle \frac{\partial \langle U_k\rangle}{\partial x_l} + G_{kl}\langle u_k u_l\rangle + \frac{3}{2} C_0 \epsilon\,, \tag{21}$$

while the corresponding exact equation (from Eq. 18) is

$$\frac{dk}{dt} = P - \epsilon\,, \tag{22}$$

where

$$P \equiv -\langle u_k u_l\rangle \frac{\partial \langle U_k\rangle}{\partial x_l}, \tag{23}$$

$$\epsilon \equiv \tfrac{1}{2}\epsilon_{ll}\,. \tag{24}$$

By comparing Eqs. (21) and (22), it may be seen that the Langevin model yields the proper evolution of k provided that G_{ij} satisfies the kinematic constraint

$$G_{kl}\langle u_k u_l\rangle + \tfrac{3}{2} C_0 \epsilon = -\epsilon\,. \tag{25}$$

For the model of Eq. (16) this constraint becomes

$$(\alpha_1 + \alpha_2 b_{ll}^2 + \tfrac{1}{2} + \tfrac{3}{4} C_0)(1/\tau) + (\gamma_1 + \beta_2 + \beta_3 + \tfrac{1}{3}\gamma^*) I_1 + \gamma^* I_2 = 0\,, \tag{26}$$

where

$$\gamma^* = \gamma_2 + \gamma_3 + \gamma_5 + \gamma_6\,, \tag{27}$$

$$b_{ll}^2 + b_{li} b_{il}\,, \tag{28}$$

$$I_1 \equiv b_{kl}\frac{\partial \langle U_k\rangle}{\partial x_l} = -\frac{1}{2\tau}\frac{P}{\epsilon}, \tag{29}$$

$$I_2 \equiv b_{ki} b_{il}\frac{\partial \langle U_k\rangle}{\partial x_l}. \tag{30}$$

This shows that it is not possible to choose constant values for all model coefficients; since this constraint contains the three invariants b_{ll}^2, I_1, and I_2, at least one coefficient must be a function of these invariants.

We satisfy Eq. (26) by letting α_2, γ_1, β_2, β_3, γ_2, γ_3, γ_5, and γ_6 remain constant. Then α_1 is given by

$$\alpha_1 = -(\tfrac{1}{2} + \tfrac{3}{4} C_0) - (\gamma_1 + \beta_2 + \beta_3 + \tfrac{1}{3}\gamma^*)\tau I_1 - \gamma^* \tau I_2 - \alpha_2 b_{ll}^2\,. \tag{31}$$

This method of satisfying Eq. (26) is not unique, but it is a reasonable choice in that α_1 remains well behaved as I_1, I_2, or b_{ll}^2 tend to zero independently. When Eq. (31) is substituted into Eq. (16), the terms containing γ_1 cancel. Then G_{ij} no longer depends on γ_1, so that γ_1 is completely arbitrary. An expedient method for removing this indeterminacy is to fix γ_1 in the following way:

$$\gamma_1 = -(\beta_2 + \beta_3 + 1/3\,\gamma^*)\,. \tag{32}$$

Then α_1 is independent of I_1 (Eq. 31). In most flows $|I_2|$ and b_{ll}^2 are both much smaller than one so that α_1 is only a weak function of the anisotropy and of I_2. Equation (31) becomes approximately

$$\alpha_1 \approx -(\tfrac{1}{2} + \tfrac{3}{4} C_0) = -2.075\,. \tag{33}$$

This shows that α_1 is nearly constant.

At this point it proves useful to rewrite the modeled Reynolds-stress equation for homogeneous flows, Eq. (17), substituting G_{ij} from Eq. (16) and including the turbulent kinetic energy constraint of Eq. (31). We replace the Reynolds stresses on the right-hand side of Eq. (17) by the normalized anisotropy tensor of Eq. (15) and decompose the mean velocity gradient into its symmetric and antisymmetric components:

$$\frac{\partial \langle U_p\rangle}{\partial x_q} = S_{pq} + R_{pq}\,, \tag{34}$$

where

$$S_{pq} \equiv \frac{1}{2}\left(\frac{\partial \langle U_p\rangle}{\partial x_q} + \frac{\partial \langle U_q\rangle}{\partial x_p}\right), \tag{35}$$

$$R_{pq} \equiv \frac{1}{2}\left(\frac{\partial \langle U_p\rangle}{\partial x_q} - \frac{\partial \langle U_q\rangle}{\partial x_p}\right). \tag{36}$$

Here S_{pq} is the mean rate of strain tensor and R_{pq} is the mean rate of rotation tensor. Equation (17) becomes

$$\frac{d\langle u_k u_l\rangle}{dt} = -2k\left(b_{ki}S_{li} + b_{li}S_{ki} + \frac{2}{3}S_{kl}\right) - 2k(b_{ki}R_{li} + b_{li}R_{ki}) - (3C_0 + 2)\epsilon b_{kl} - \frac{2}{3}\epsilon\delta_{kl}$$

$$+ 4g_1\epsilon\left[\tfrac{1}{3}b_{kl} + b_{ki}b_{il} - b_{ii}^2(b_{kl} + \tfrac{1}{3}\delta_{kl})\right] + 2g_2\, k\left[\tfrac{2}{3}S_{kl} + S_{ki}b_{il} + S_{li}b_{ik} - 2I_1(b_{kl} + \tfrac{1}{3}\delta_{kl})\right]$$
$$+ 2g_3 k b_{is}(S_{sk}b_{il} + S_{sl}b_{ik}) + 4g_4 k S_{is}b_{ks}b_{il} + \tfrac{2}{3}(g_3 + g_4)k\left[b_{ls}S_{sk} + b_{ks}S_{sl} - 2(I_1 + 3I_2)(b_{kl} + \tfrac{1}{3}\delta_{kl})\right]$$
$$+ 2g_5\, k(R_{ki}b_{il} + R_{li}b_{ik}) + 2g_6 k b_{is}(R_{sk}b_{il} + R_{sl}b_{ik}), \tag{37}$$

where

$$g_1 = \alpha_2, \quad g_2 = \beta_2 + \beta_3, \quad g_3 = \gamma_2 + \gamma_3, \quad g_4 = \gamma_5 + \gamma_6, \quad g_5 = \beta_2 + \tfrac{1}{3}(\gamma_2 + \gamma_6) - \beta_3 - \tfrac{1}{3}(\gamma_3 + \gamma_5), g_6 = \gamma_3 - \gamma_2. \tag{38}$$

Note that only six linearly independent groupings of the model coefficients appear in Eq. (37).

B. Fluctuating pressure-rate-of-strain correlation

In second-order closures, it is necessary to model the term ϕ_{ij} of Eqs. (18) and (19) in terms of the local mean quantities $\langle u_k u_l\rangle$, $\partial\langle U_p\rangle/\partial x_q$, and ϵ. This usually proceeds by writing the exact integral solution for this term as derived by Chou.[36] For homogeneous flows with uniform mean velocity gradients,

$$\phi_{ij} = \phi_{ij}^{(1)} + \phi_{ij}^{(2)}, \tag{39}$$

where

$$\phi_{ij}^{(1)} = \frac{\partial\langle U_l\rangle}{\partial x_m} A_{milj}, \tag{40}$$

$$A_{milj} = -\frac{1}{2\pi}\int_{\text{vol}} \frac{\partial^2\langle u_m(\mathbf{y})u_i(\mathbf{x})\rangle}{\partial r_l\,\partial r_j}\frac{1}{r}\,d\mathbf{y}, \tag{41}$$

$$\phi_{ij}^{(2)} = -\frac{1}{4\pi}\int_{\text{vol}} \frac{\partial^3\langle u_l(\mathbf{y})u_m(\mathbf{y})u_i(\mathbf{x})\rangle}{\partial r_l\,\partial r_m\,\partial r_j}\frac{1}{r}\,d\mathbf{y}, \tag{42}$$

$$\mathbf{y} = \mathbf{x} + \mathbf{r}, \quad r = |\mathbf{r}|. \tag{43}$$

It is then straightforward to derive the following kinematic constraints on A_{milj} (see Ref. 37):

$$A_{milj} = A_{imlj}, \quad A_{milj} = A_{mijl}, \qquad A_{mili} = 0, \quad A_{mijj} = 2\langle u_m u_i\rangle. \tag{44}$$

The term $\phi_{ij}^{(1)}$ is called the rapid pressure term since it responds instantly to changes in the mean velocity gradients, while $\phi_{ij}^{(2)}$ is often referred to as the "slow" pressure term or as the "return-to-isotropy" term.

Since the mean velocity gradients do not appear explicitly in $\phi_{ij}^{(2)}$, it is customary to model this term as a function of $\langle u_k u_l\rangle$ and ϵ only.[2,3] This implies that the only effect of $\partial\langle U_p\rangle/\partial x_q$ on $\phi_{ij}^{(2)}$ is an indirect effect, via its influence on $\langle u_k u_l\rangle$ and ϵ. Recently Jones and Musonge[38] derived the evolution equation for the term analogous to $\phi_{ij}^{(2)}$ that appears in the scalar flux transport equation, demonstrating that this term does in fact depend on the mean velocity gradients. The evolution equation for $\phi_{ij}^{(2)}$ is derived similarly and leads to the same conclusion. They then argue that since both terms (here $\phi_{ij}^{(1)}$ and $\phi_{ij}^{(2)}$) depend on the mean velocity gradients, there is little to be gained by modeling these terms separately.

We feel that this point merits further consideration. The assumption of an equilibrium structure is implicit in any closure model, in order that unknown quantities can be expressed in terms of known quantities. In any one-point closure for constant property homogeneous flows, all turbulence structure must be expressed in terms of $\langle u_k u_l\rangle$, $\partial\langle U_p\rangle/\partial x_q$, and ϵ. Explicit dependence on the mean velocity gradients would be excluded from the modeling of $\phi_{ij}^{(2)}$ only if the analytic expression for $\phi_{ij}^{(2)}$ were independent of $\partial\langle U_p\rangle/\partial x_q$ or if there were a valid physical argument for excluding dependence on $\partial\langle U_p\rangle/\partial x_q$ in a particular flow that we wish to model. Jones and Musonge's solution shows that $\partial\langle U_p\rangle/\partial x_q$ does enter the evolution equation for $\phi_{ij}^{(2)}$. It is true that $\phi_{ij}^{(2)}$ does not respond instantly to changes in $\partial\langle U_p\rangle/\partial x_q$ as does $\phi_{ij}^{(1)}$; $\phi_{ij}^{(2)}$ depends, rather, on the history of $\partial\langle U_p\rangle/\partial x_q$. Lumley[39] makes the valid point that if $\phi_{ij}^{(2)}$ is expressed as a function of the mean velocity gradients as well as of $\langle u_k u_l\rangle$ and ϵ, then it will behave incorrectly in the case of an arbitrary turbulence field interacting with a suddenly imposed arbitrary mean velocity field. He also points out that Eq. (42) shows that $\phi_{ij}^{(2)}$ depends only on the fluctuating velocity field. In constructing closure models for $\phi_{ij}^{(2)}$, there is some incentive, then, for excluding $\partial\langle U_p\rangle/\partial x_q$ on the grounds that the resulting model may be applicable to a wider class of flows than a model that includes $\partial\langle U_p\rangle/\partial x_q$.

On the other hand, in flows where $\partial\langle U_p\rangle/\partial x_q$ changes by a relatively small amount (magnitude changes of order $1/\tau$) or where $\partial\langle U_p\rangle/\partial x_q$ changes relatively slowly (on a time scale of order τ), then the current value of $\partial\langle U_p\rangle/\partial x_q$ provides an adequate representation of its recent history. Excluding the mean velocity gradients from the modeling of $\phi_{ij}^{(2)}$ may exclude a physical mechanism that the exact evolution equation for $\phi_{ij}^{(2)}$ shows to be present in these flows. Moreover, there appears to be no strong reason for the two-point velocity correlations in Eq. (42), even though they are functions of the fluctuating velocities only, to be functions of the one-point quantities $\langle u_k u_l\rangle$ and ϵ only, independent of $\partial\langle U_p\rangle/\partial x_q$. Indeed, such a restriction may limit the applicability of the model in the slowly evolving flows discussed above.

It is not clear which modeling philosophy leads to the more generally applicable model. We feel that in the context of one-point closures with only $\langle u_k u_l\rangle$, $\partial\langle U_p\rangle/\partial x_q$, and ϵ available, it may be overly restrictive to exclude $\partial\langle U_p\rangle/\partial x_q$ from the modeling of $\phi_{ij}^{(2)}$. We thus reject the notion that $\phi_{ij}^{(2)}$ should be modeled as independent of the mean velocity gradients. In so doing we recognize that there may be spurious contributions to $\phi_{ij}^{(2)}$ in rapidly evolving mean flow fields, although it should be pointed out that we are still able to deal

with the rapid distortion of initially isotropic turbulence as discussed below. (If we did wish to express $\phi_{ij}^{(2)}$ as a function of $\langle u_k u_l \rangle$ and ϵ only, H_{ijkl} of Eq. 16 and A_{milj} of Eq. 41 would be related by $H_{ijkl} = \langle u_p u_j \rangle^{-1} A_{lpki}$. Applying the kinematic constraints of Eq. 44 would then uniquely determine all nine model constants in H_{ijkl}.)

C. Rapid distortion of initially isotropic turbulence

We now consider the rapid distortion of initially isotropic turbulence by uniform mean velocity gradients. This is not inconsistent with the discussion above concerning $\phi_{ij}^{(2)}$ since $\phi_{ij}^{(2)}$ is identically zero in the initially isotropic turbulence.

Rapid distortion theory is rigorously justified only in cases where the time scale of the mean strain $T = \| \partial \langle U_p \rangle / \partial x_q \|^{-1}$ is much smaller than the turbulence time scale τ (see Refs. 40–42). If T is smaller than τ_η as well as being much smaller than τ, then even the smallest scales would be deformed to the extent that local isotropy no longer prevailed. Clearly, such flows are beyond the scope of our model. However, rapid distortion theory has been applied to many experiments in irrotational deformations of homogeneous turbulence, sometimes including corrections for decay or for the initial anisotropy.[41–46] These are flows in which the time scale ratio τ/T is of order unity, yet this linear theory successfully models the initial stages of the deformation. Hence this is a reasonable constraint to apply to our model.

We set b_{kl} equal to zero in Eq. (37) and retain only those terms involving the mean velocity gradients. The model reduces to

$$\frac{d \langle u_k u_l \rangle}{dt} = \frac{4k}{3} (g_2 - 1) S_{kl} , \tag{45}$$

while rapid distortion theory applied to the exact Reynolds-stress evolution equation (Eq. 18) yields[34]

$$\frac{d \langle u_k u_l \rangle}{dt} = - \frac{8k}{15} S_{kl} . \tag{46}$$

The Langevin model is then compatible with rapid distortion theory provided that

$$g_2 = \beta_2 + \beta_3 = \tfrac{3}{5} . \tag{47}$$

Further constraints are deduced by considering the fourth-order tensor H_{ijkl} of Eq. (16) directly. In isotropic turbulence, H_{ijkl} is an isotropic tensor (i.e., it involves only combinations of Kronecker deltas δ_{ij}). The slow pressure term $\phi_{ij}^{(2)}$) is identically equal to zero, so that H_{ijkl} is related to A_{limj} of Eq. (41) by

$$H_{ijkl} = \langle u_p u_j \rangle^{-1} A_{lpki} . \tag{48}$$

We emphasize that Eq. (48) holds only in isotropic turbulence; $\phi_{ij}^{(2)}$ is not being modeled as independent of $\partial \langle U_p \rangle / \partial x_q$. With b_{kl} identically equal to zero and $\langle u_k u_l \rangle = 2/3\, k \delta_{kl}$, the four kinematic constraints of Eq. (44) lead to

$$\beta_1 = - \tfrac{1}{5} , \tag{49}$$

$$\beta_2 = \tfrac{4}{5} , \tag{50}$$

$$\beta_3 = - \tfrac{1}{5} . \tag{51}$$

These values are consistent with Eq. (47). Coefficient β_1 does not affect G_{ij} in constant property flows ($\partial \langle U_l \rangle / \partial x_l = 0$, Eq. 16), hence the evolution of the Reynolds stresses is independent of the value of β_1; β_2 and β_3 appear in the modeled Reynolds-stress equation (Eq. 37) only as $g_2 = \beta_2 + \beta_3$ and as part of g_5. As far as the evolution of the Reynolds stresses is concerned, then, Eq. (47) is the only relevant isotropic rapid distortion constraint.

D. Two-dimensional limit

A two-dimensional state in which one of the eigenvalues of the Reynolds-stress tensor is identically zero is attainable only as an initial condition for the Langevin model. This is evident from the presence of the term containing C_0 in the modeled pdf evolution equation, Eq. (9); this term represents a diffusion in velocity space. True two-dimensional states, in which one component of the fluctuating velocity is identically zero in the principal axes of $\langle u_k u_l \rangle$, violate local isotropy and are beyond the scope of this model. However, there are conditions under which one eigenvalue of the Reynolds-stress tensor becomes much smaller than the other two while local isotropy still exists. Such states are approached experimentally in homogeneous flows in axisymmetric contractions and some plane distortions.[42,46] Similar effects are expected in inhomogeneous flows. The Langevin model should work in these cases, so it is reasonable to apply a constraint that is rigorous only in the two-dimensional limit.

By considering arbitrary time-dependent translations and rotations of reference frame, Speziale[47] has derived a transformation rule for the Reynolds-stress evolution equation in two-dimensional flows that shows explicitly the effects of the antisymmetric components of the mean velocity gradients R_{pq} (Eq. 36). He concludes that the only terms in a modeled Reynolds-stress equation that contain R_{pq} are (in the two-dimensional limit)

$$\frac{\partial \langle u_k u_l \rangle}{\partial t} + \langle U_i \rangle \frac{\partial \langle u_k u_l \rangle}{\partial x_i} = \langle u_i u_k \rangle R_{li} + \langle u_i u_l \rangle R_{ki} + (\text{terms independent of } R_{pq}) . \tag{52}$$

The terms in R_{pq} in Eq. (52) result from the production terms and the modeled fluctuating pressure gradient-velocity correlation terms in Eq. (12). The Langevin model, Eq. (37), yields (for homogeneous flows)

$$\begin{aligned} \frac{d \langle u_k u_l \rangle}{dt} = {} & (g_5 - 1 + \tfrac{2}{3} g_6) [\langle u_i u_k \rangle R_{li} + \langle u_i u_l \rangle R_{ki}] \\ & + g_6 (1/2k) [\langle u_i u_s \rangle \langle u_i u_l \rangle R_{sk} \\ & + \langle u_i u_s \rangle \langle u_i u_k \rangle R_{sl}] \\ & + (\text{terms independent of } R_{pq}) , \end{aligned} \tag{53}$$

where we have expressed the right-hand side of Eq. (37) in terms of the Reynolds stresses.

Consider a homogeneous two-dimensional turbulence in the $x_1 - x_2$ plane. Then the convective derivative in Eq. (52) becomes a simple time derivative. The only nonzero components of the Reynolds-stress tensor are $\langle u_1^2 \rangle$, $\langle u^2 \rangle$, and $\langle u_1 u_2 \rangle = \langle u_2 u_1 \rangle$. The mean velocity gradients are confined to the $x_1 - x_2$ plane and are uniform so that the most

general form for R_{pq} is $R_{12} = -R_{21}$, where R_{12} is spatially uniform and all other components of R_{pq} are zero. It is then straightforward to show that the effect of R_{pq} on the evolution of the Reynolds stresses according to the model (Eq. 53) is the same as that given by Speziale's transformation rule (Eq. 52), provided that

$$g_5 - \tfrac{1}{3}g_6 = 2. \tag{54}$$

E. Indeterminacy

For constant property flows ($\partial \langle U_l \rangle / \partial x_l = 0$), Eq. (16) shows that neither β_1 nor γ_4 have any effect on G_{ij}. Here β_1 was found by considering the rapid distortion of initially isotropic turbulence (Eq. 49) while γ_4 remains arbitrary. We can set γ_4 to any value in order to remove this indeterminacy, but there is no reason to choose a value different than zero:

$$\gamma_4 = 0. \tag{55}$$

F. Summary

The above analysis has removed seven degrees of freedom from the model (Eqs. 31, 32, 49–51, 54, and 55) leaving four degrees of freedom to be determined. No additional constraints were found by considering the fluctuating pressure-rate-of-strain correlation. The two "extreme state" constraints, Eqs. (47) and (54), should be regarded as tentative. They apply to states of turbulence at the limits of applicability of this model, and if satisfying them led to unacceptable evolution of the Reynolds stresses in the flows considered in Sec. V below, we could remove them without serious loss of model integrity. We also note that these constraints apply rigorously only in their respective extreme states; we take them as fixed for all turbulence states because we seek constant values for the model coefficients.

V. CHOICE OF MODEL CONSTANTS

With α_1 given by Eq. (31), all other model coefficients can be constant without violating the constraints derived above. Four degrees of freedom remain to be determined: g_1, g_3, g_4, and g_5 (g_2 is given by Eq. 47, g_6 by Eq. 54). We now fix these four constants by optimizing their values with respect to experimental data in homogeneous flows with uniform mean velocity gradients. The optimization method is outlined first, followed by a discussion of the relevant experimental data.

A. Numerical optimization

In homogeneous flows it is common practice to use the smallest amount of experimental data in the simplest possible flow configurations in order to fix the model constants.[1–3] Algebraic methods are often used in which the modeled Reynolds–stress evolution equations are matched to experimental data at a single point in each flow. This results in a matrix equation to be solved for the model constants, but the method is ill-conditioned if there are more data to be matched than there are model constants. If the principal goal of the exercise is to assess the predictive capabilities of a model in homogeneous flows, then the algebraic method is a good one since the least possible amount of experimental data is used to fix the model constants.

We are considering the special case of constant property, homogeneous turbulence in order to calibrate a model that will eventually be applied to variable density in homogeneous flows. We therefore wish to use the maximum amount of information that can be extracted from experimental data in homogeneous flows, that is, the full time evolution of the Reynolds stresses in as many different types of flows as possible. This is done by finding the set of M constants $\mathbf{C} = \{C_1, C_2, \ldots, C_M\}$ that minimizes the difference between the model calculations and the experimental data. More precisely, we define an error measure $e = e(\mathbf{C})$ to be the difference between the modeled evolution of $\langle u_k u_l \rangle$ and N sets of experimental Reynolds-stress data. For a given $\mathbf{C}$ the modeled evolution equations are integrated N times with initial conditions appropriate to each experiment, and then $e(\mathbf{C})$ is computed. We find the $\mathbf{C}$ that minimizes $e(\mathbf{C})$ by searching the $\mathbf{C}$ space according to a pattern search optimization algorithm as contained in standard texts on nonlinear programming (Ref. 48, for example).

For each experiment the Reynolds-stress data ($\langle u_k u_l \rangle$ as a function of time t) are reduced to a set of least-squares cubic splines coefficients.[49] The mean flow field ($\partial \langle U_p \rangle / \partial x_q$) is specified, initial conditions for the modeled Reynolds stresses are matched to the splined data at $t = 0$, and $\tau = k/\epsilon$ is evaluated directly from the spline coefficients for all t using the homogeneous turbulent kinetic energy equation (Eq. 22):

$$\tau = \frac{k}{P - dk/dt}. \tag{56}$$

The modeled Reynolds-stress equations (Eq. 17) with G_{ij} given by Eq. (16) are integrated using a fourth-order Runge–Kutta method. A pattern search optimization algorithm is used to minimize a weighted root-mean-square error over the seven quantities k, b_{11}, b_{22}, b_{33}, $b_{12} = b_{21}$, $b_{13} = b_{31}$, and $b_{23} = b_{32}$ for N sets of experimental data, subject to the constraints derived in Sec. IV. Since this is a least-squares method, there is no potential for over-constraining the model constants.

Our optimizations were performed on a VAX 11-750 using UNIX FORTRAN. For a four-dimensional coefficient space and twelve sets of experimental data, the evaluation of $e(\mathbf{C})$ for each coefficient set $\mathbf{C}$ required about 1½ CPU min. A typical optimization converges to a local minimum of $e(\mathbf{C})$ in 100–500 iterations, depending on the starting point in coefficient space. With the basic algorithm in place, different models can be optimized with a minimum of new coding.

B. Experimental data

For our purposes experiments involving homogeneous turbulence in the presence of uniform mean velocity gradients can be divided into three categories based on the mean velocity gradients and the normalized anisotropy tensor:

(1) irrotational strains in which the principal axes of b_{kl} are aligned with those of $\partial \langle U_p \rangle / \partial x_q$;

(2) irrotational strains in which the principal axes of b_{kl} are not aligned with those of $\partial \langle U_p \rangle / \partial x_q$; and

(3) homogeneous shear flows.

These are convenient classifications since different sets of model constants are relevant in each case. We now present several sets of experimental data representing each of the three categories; these data are used in the numerical optimizations. In all pure strain cases ($R_{pq} \equiv 0$), we consider a coordinate system that coincides with the principal axes of the mean velocity gradients with x_1 in the streamwise direction. For the shear flows, x_1 is the streamwise direction and x_2 is the direction in which $\langle U_1 \rangle$ increases. Experimental data in decaying turbulence ($\partial \langle U_p \rangle / \partial x_q \equiv 0$) are not used to determine the values of the model constants. A discussion of decaying turbulence and solid body rotation is deferred to Sec. VI.

(1) Irrotational strain, principal axes of b_{kl} aligned with those of $\partial \langle U_p \rangle / \partial x_q$

The mean rate of rotation R_{pq} is identically zero and only the diagonal components of b_{kl} are nonzero in these flows. The only groupings of constants that enter the modeled Reynolds-stress equations are g_1, g_2, and $g_3 + g_4$. Several types of experiments fall under this general heading.

Axisymmetric contractions are characterized by $S_{11} = D, S_{22} = S_{33} = -D/2$. Many workers have presented data in such flows (Refs. 42 and 46, for example). Of these, only Tucker[42] used a duct for which D remains constant through the contraction. Still, using Eq. (22) to determine ϵ gives negative values of ϵ over approximately the final 25% of the deformation; the data of Mills and Corrsin[46] exhibit similar behavior. We thus reject axisymmetric contraction data for use in the optimization, but we do model the first 70% of Tucker's data using the optimum set of model constants in order to evaluate the model's performance in these flows.

A second subclass of irrotational strains is the transverse irrotational plane strain in which $\langle U_1 \rangle$ remains constant: $S_{11} = 0$, $S_{22} = -S_{33} = D$ in this case. Gence[44] and Gence and Mathieu[45] present a series of experiments in which turbulence is subjected to two simultaneous deformations, the second rotated by an angle α with respect to the first. Two sets of their data, $\alpha = 0$ and $\alpha = \pi/2$, are taken as typical of these flows. A third experiment, that of Tucker and Reynolds[43] (also in Ref. 42), is used as well.

A case similar to the above is the longitudinal plane strain or two-dimensional contraction in which the streamwise direction lies in the plane of the mean strain: $S_{11} = -S_{33} = D, S_{22} = 0$. The model, being oblivious to the mean velocity, treats this as identical to the case above in which the plane of the mean strain is normal to the streamwise direction. Nevertheless, two examples of such flows (Tucker[42]) are included for completeness.

The last subclass of flows in this category is the axisymmetric expansion, in which $S_{11} = -D$, $S_{22} = S_{33} = D/2$. Such flows are not generally created in the laboratory since the adverse streamwise pressure gradient leads to flow separation. Tucker[42] studies instead an "equivalent symmetric diffuser" in which $S_{11} = S_{22} = D/2$, $S_{33} = -D$. We use his data as representative of this type of flow. Assuming that only gradients of the mean velocity and not the mean velocity itself affect the turbulence, this flow is expected to be structurally similar to the axisymmetric expansion.

In each of the above seven flows, initial conditions are set at the first reported data point where D becomes constant. For the Gence and Mathieu $\alpha = \pi/2$ case, the second reported data point in the second distortion is taken as the initial condition since we expect that the turbulence does not feel the effect of the new orientation of the mean strain until a distance of one integral scale $L \equiv k^{3/2}/\epsilon$ into the second duct.

(2) Irrotational strain, principal axes of b_{kl} not aligned with those of $\partial \langle U_p \rangle / \partial x_q$

Again, R_{pq} is identically zero in this category. We use three sets of Gence and Mathieu's data[44,45] as typical of these flows: $\alpha = \pi/8$, $\alpha = \pi/4$, and $\alpha = 3\pi/8$. Here $S_{11} = 0$, $S_{22} = -S_{33} = D$, and $b_{23} = b_{32}$ is now nonzero in addition to the three diagonal components of b_{kl}; g_1, g_2, g_3, and g_4 enter the modeled Reynolds-stress equations. Initial conditions are set at the second reported data point in the second distortion as for the $\alpha = \pi/2$ case above.

(3) Homogeneous shear flows

The only nonzero component of $\partial \langle U_p \rangle / \partial x_q$ is $\partial \langle U_1 \rangle / \partial x_2 = D = \text{const}$. Then $S_{12} = S_{21} = D/2$, $R_{12} = -R_{21} = D/2$, and all other components of S_{pq} and of R_{pq} are zero. Here $b_{12} = b_{21}$ is nonzero in addition to the three diagonal components of b_{kl}. All six groupings of model constants $g_1 - g_6$ affect the evolution of the Reynolds stresses in these flows.

It is observed that experiments in homogeneous turbulent shear flows fall into two general categories: weakly sheared flows in which $\langle u_k u_l \rangle$ and k reach asymptotic constant values, and strongly sheared flows in which $\langle u_k u_l \rangle$ and k grow exponentially. Karnik[50] concludes that in either case, the normalized Reynolds stresses or the normalized anisotropy tensor b_{kl} approach asymptotic quasi-universal values independent of the value of the mean shear:

$$b_{kl_{\text{asym}}} = \begin{bmatrix} 0.21 \pm 0.038 & -0.16 \pm 0.008 & 0 \\ -0.16 \pm 0.008 & -0.13 \pm 0.018 & 0 \\ 0 & 0 & -0.07 \pm 0.025 \end{bmatrix}. \tag{57}$$

It can be shown from Eq. (37) that the term multiplying g_6 in the modeled Reynolds-stress equations for these flows is equal to b_{33} times the term multiplying g_5. Equation (57) shows that b_{33} is approximately equal to -0.07 for all homogeneous shear flows. Therefore, the terms containing g_6 are small compared to the terms containing g_5 in the mo-

deled equations. It is this fact that allows us to apply Speziale's constraint (Eq. 54) without significantly affecting the evolution of the Reynolds stresses in all flows considered here (g_5 and g_6 enter the modeled Reynolds-stress equation only for $R_{pq} \neq 0$).

We take three sets of experimental data as typical of these flows. Champagne, Harris, and Corrsin[51] is an example of a weakly sheared flow while Harris, Graham, and Corrsin[52] and Tavoularis and Corrsin[32] are examples of strongly sheared flows. In each case initial conditions are set at the first reported data point downstream of where the experimenters claim that a reasonable degree of transverse homogeneity is attained.

C. Summary

The four remaining model constants g_1, g_3, g_4, and g_5 (six without the two "extreme state" constraints) are optimized with respect to twelve sets of experimental data in homogeneous flows with uniform mean velocity gradients. Each of the coefficient groups $g_1 - g_6$ of Eq. (38) enters the modeled equations for at least some of the flow types considered, although the dependence on g_6 is weak. A standard optimization algorithm is used to minimize the difference between the modeled evolution of k and b_{kl} and experimental data.

The most severe test of the model is expected in flows of the second category above where the principal axes of b_{kl} must adjust significantly to the mean velocity gradients. This is especially true in view of the modeling of $\phi_{ij}^{(2)}$ discussed in Sec. IV. By the time that most experiments in homogeneous shear flows achieve transverse homogeneity, there is virtually no further evolution of b_{kl} at all. Still, it is of interest to see how the model performs in both the weakly sheared and the strongly sheared cases; many second-order closure models cannot deal with both cases equally well.

VI. PERFORMANCE OF THE MODEL IN HOMOGENEOUS FLOWS

A set of optimum model constants is presented and the modeled evolution of k and b_{kl} is compared to experimental data in each of the thirteen flows considered in Sec. V. The qualitative behavior of the model in two other important classes of homogeneous flows, decaying turbulence and solid body rotation, is also examined.

Optimizations were performed both with and without the "extreme state" constraints, Eqs. (47) and (54). Those performed without Eq. (47) yield $g_2 \approx 0.63$ as optimum, thus nearly recovering the rapid distortion constraint $g_2 = 0.60$. Those performed without Eq. (54) do not converge to a unique optimum value of g_6 for all reasonable starting points in coefficient space (C_i of order unity, $i = 1,...,M$). This verifies that the modeled evolution of the Reynolds stresses for the experiments considered is a very weak function of g_6, as anticipated. We conclude that the constraints of Eqs. (47) and (54) can be applied without adversely affecting the evolution of the Reynolds stresses in homogeneous flows.

The optimum values of g_1, g_3, g_4, and g_5 are found to be

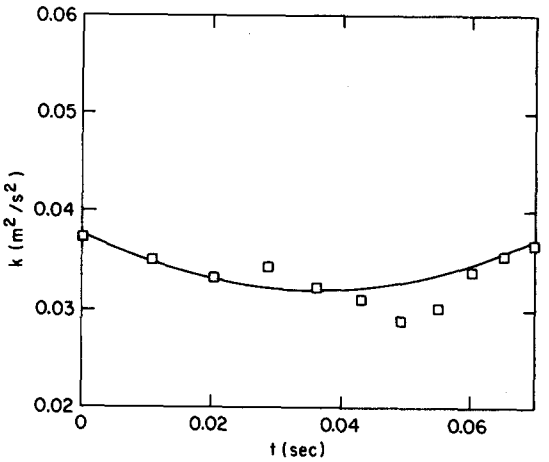

FIG. 1. Evolution of turbulent kinetic energy k for the axisymmetric contraction experiment of Tucker,[42] $D = 13.71$/sec. Langevin model calculations (lines), experimental data (symbols).

$$g_1 = 3.7, \quad g_3 = 0.83, \quad g_4 = 1.2, \quad \text{and} \quad g_5 = 0.27. \tag{58}$$

Using the definitions of $g_1 - g_6$ in Eq. (38) and the six constraints of Eqs. (32), (49)–(51), (54), and (55), we then find the optimum values for the 10 model constants:

$$\begin{aligned} &\alpha_2 = 3.7, \quad \beta_1 = -0.20, \quad \beta_2 = 0.80, \quad \beta_3 = -0.20, \\ &\gamma_1 = -1.28, \quad \gamma_2 = 3.01, \quad \gamma_3 = -2.18, \\ &\gamma_4 = 0.00, \quad \gamma_5 = 4.29, \quad \gamma_6 = -3.09, \end{aligned} \tag{59}$$

and α_1 is given by Eq. (31). For the 13 experiments considered, α_1 varies between -1.2 and -3.0, but is usually between -2.1 and -2.3. This verifies the approximation given in Eq. (33).

The modeled evolution of k and b_{kl} using these optimum model constants versus 13 sets of experimental data is shown in Figs. 1–26. In all cases except one the modeled k agrees quite well with experimental data. This is to be expected, since τ is extracted directly from the data. For Tucker's longitudinal plane strain, duct 2 (Fig. 6), the model gives too large a value of k near the downstream end of the distortion. From Eqs. (15) and (22) and the discussion of

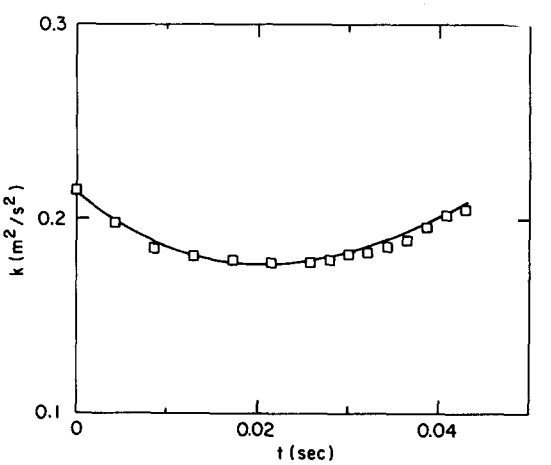

FIG. 2. Evolution of turbulent kinetic energy k for the transverse plane strain experiment of Gence and Mathieu,[44,45] $\alpha = 0$, $D = 32.23$/sec. Lines and symbols are the same as in Fig. 1.

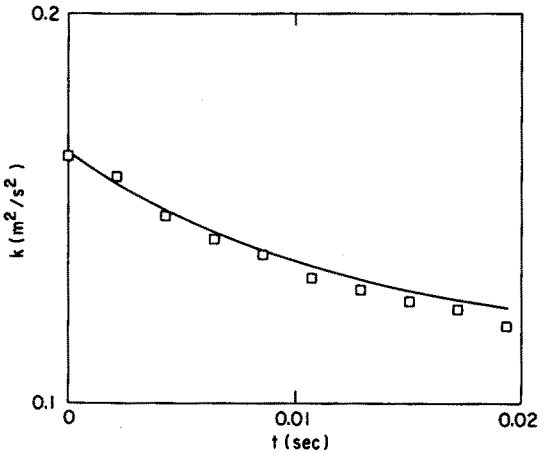

FIG. 3. Evolution of turbulent kinetic energy k for the transverse plane strain experiment of Gence and Mathieu,[44,45] $\alpha = \pi/2$, $D = -32.23$/sec. Lines and symbols are the same as in Fig. 1.

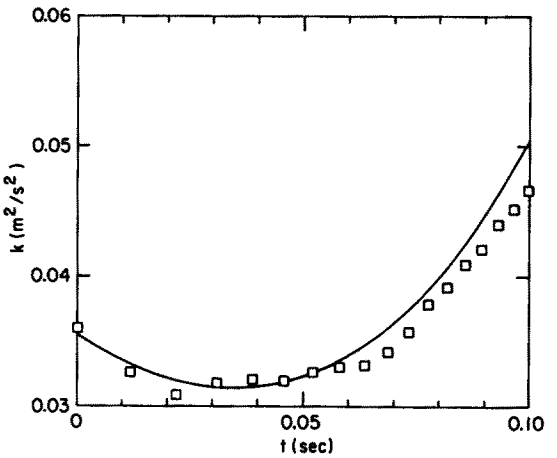

FIG. 6. Evolution of turbulent kinetic energy k for the longitudinal plane strain experiment of Tucker,[42] duct 2, $D = 14.21$/sec. Lines and symbols are the same as in Fig. 1.

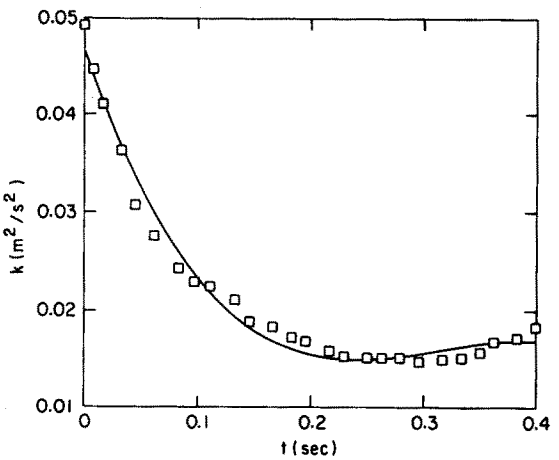

FIG. 4. Evolution of turbulent kinetic energy k for the transverse plane strain experiment of Tucker and Reynolds,[43] $D = 4.45$/sec. Lines and symbols are the same as in Fig. 1.

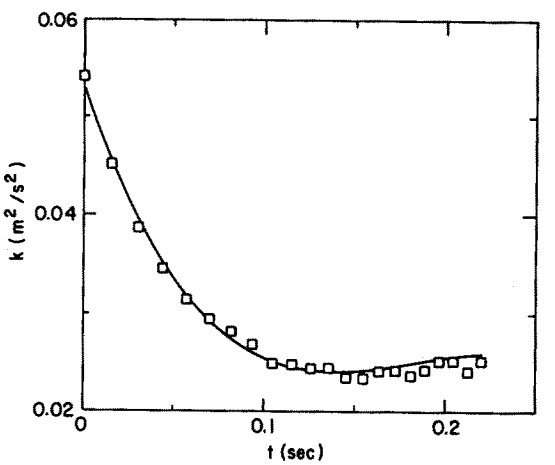

FIG. 7. Evolution of turbulent kinetic energy k for the equivalent symmetric diffuser experiment of Tucker,[42] $D = 7.12$/sec. Lines and symbols are the same as in Fig. 1.

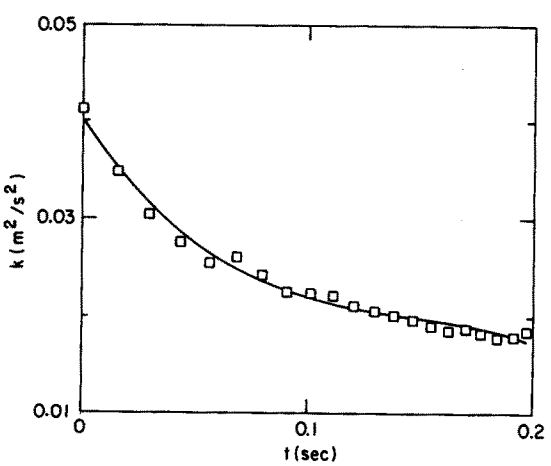

FIG. 5. Evolution of turbulent kinetic energy k for the longitudinal plane strain experiment of Tucker,[42] duct 3, $D = 4.63$/sec. Lines and symbols are the same as in Fig. 1.

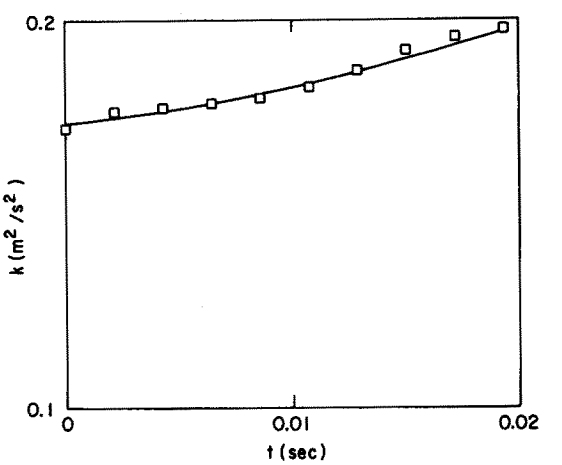

FIG. 8. Evolution of turbulent kinetic energy k for the transverse plane strain experiment of Gence and Mathieu,[44,45] $\alpha = \pi/8$, $D = 32.23$/sec. Lines and symbols are the same as in Fig. 1.

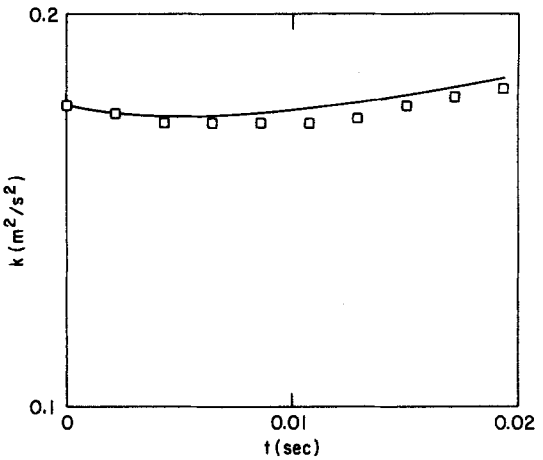

FIG. 9. Evolution of turbulent kinetic energy k for the transverse plane strain experiment of Gence and Mathieu,[44,45] $\alpha = \pi/4$, $D = 32.23$/sec. Lines and symbols are the same as in Fig. 1.

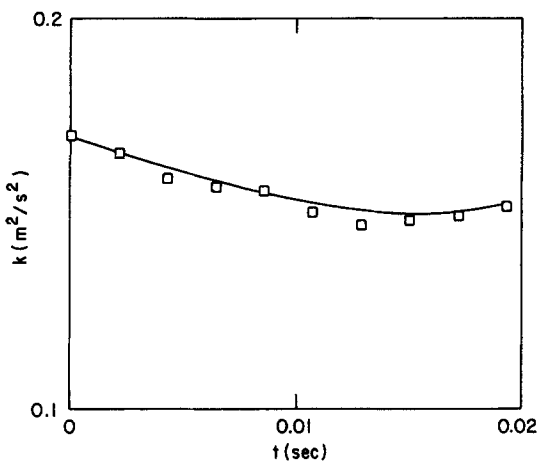

FIG. 10. Evolution of turbulent kinetic energy k for the transverse plane strain experiment of Gence and Mathieu,[44,45] $\alpha = 3\pi/8$, $D = 32.23$/sec. Lines and symbols are the same as in Fig. 1.

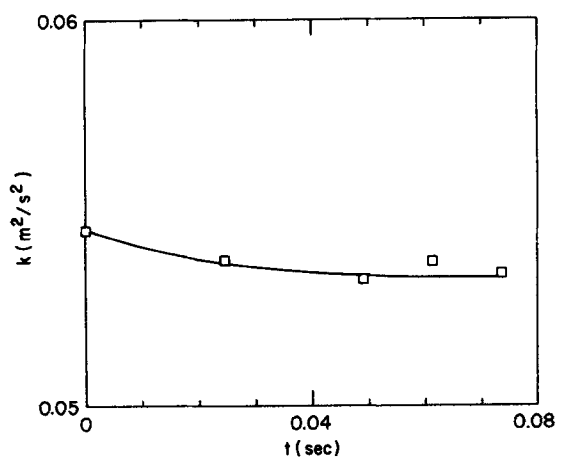

FIG. 11. Evolution of turbulent kinetic energy k for the homogeneous shear flow experiment of Champagne *et al.*,[51] $D = 12.9$/sec. Lines and symbols are the same as in Fig. 1.

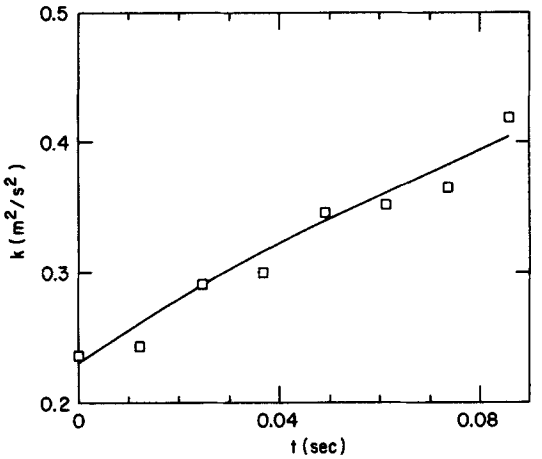

FIG. 12. Evolution of turbulent kinetic energy k for the homogeneous shear flow experiment of Harris *et al.*,[52] D = 44.0/sec. Lines and symbols are the same as in Fig. 1.

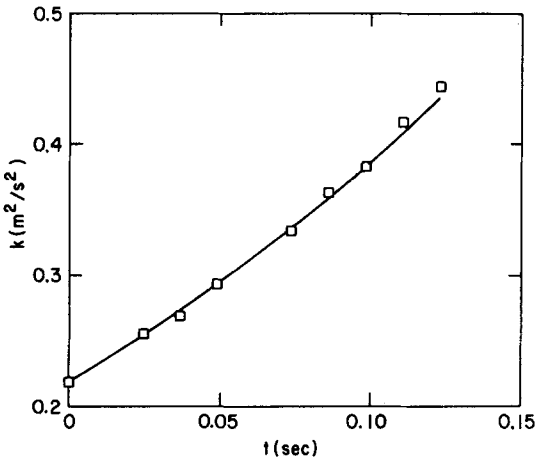

FIG. 13. Evolution of turbulent kinetic energy k for the homogeneous shear flow experiment of Tavoularis and Corrsin,[32] $D = 46.8$/sec. Lines and symbols are the same as in Fig. 1.

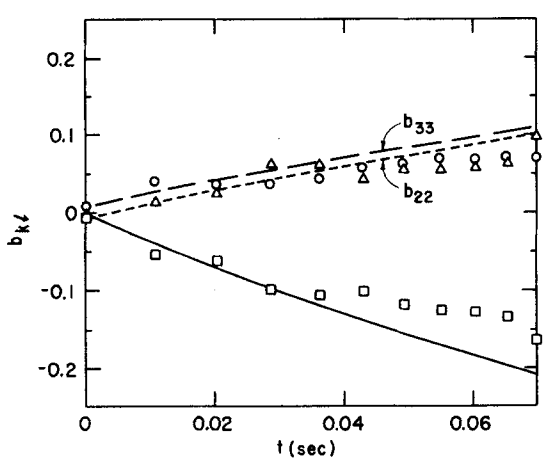

FIG. 14. Evolution of anisotropies b_{kl} for the axisymmetric contraction experiment of Tucker,[42] $D = 13.71$/sec. Langevin model calculations (lines), experimental data (symbols): □, b_{11}; △, b_{22}; ○, b_{33}.

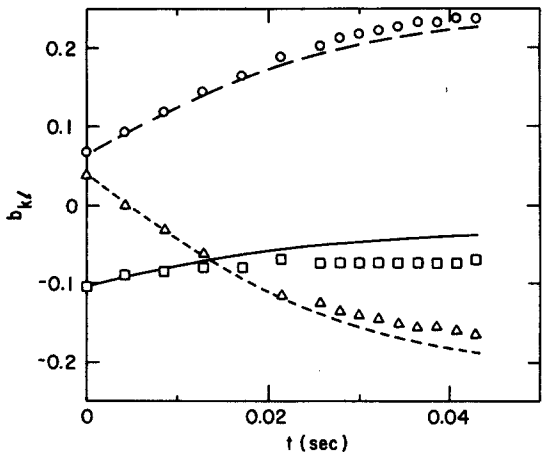

FIG. 15. Evolution of anisotropies b_{kl} for the transverse plane strain experiment of Gence and Mathieu,[44,45] $\alpha = 0$, $D = 32.23$/sec. Lines and symbols are the same as in Fig. 14.

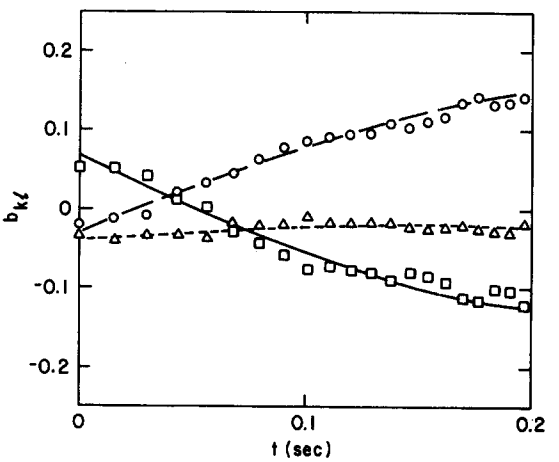

FIG. 18. Evolution of anisotropies b_{kl} for the longitudinal plane strain experiment of Tucker,[42] duct 3, $D = 4.63$/sec. Lines and symbols are the same as in Fig. 14.

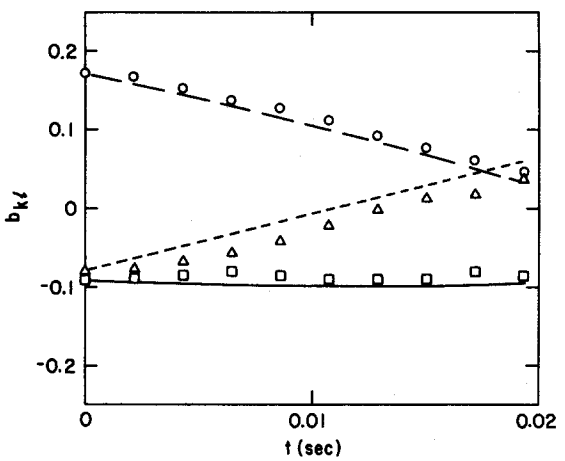

FIG. 16. Evolution of anisotropies b_{kl} for the transverse plane strain experiment of Gence and Mathieu,[44,45] $\alpha = \pi/2$, $D = -32.23$/sec. Lines and symbols are the same as in Fig. 14.

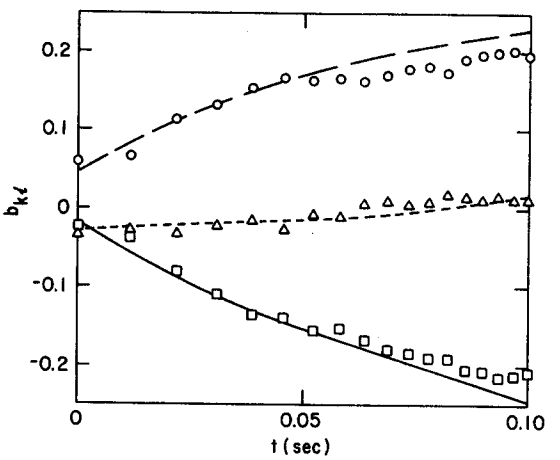

FIG. 19. Evolution of anisotropies b_{kl} for the longitudinal plane strain experiment of Tucker,[42] duct 2, $D = 14.12$/sec. Lines and symbols are the same as in Fig. 14.

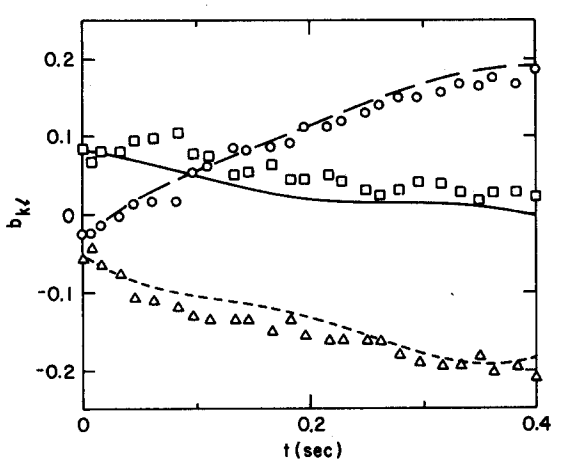

FIG. 17. Evolution of anisotropies b_{kl} for the transverse plane strain experiment of Tucker and Reynolds,[43] $D = 4.45$/sec. Lines and symbols are the same as in Fig. 14.

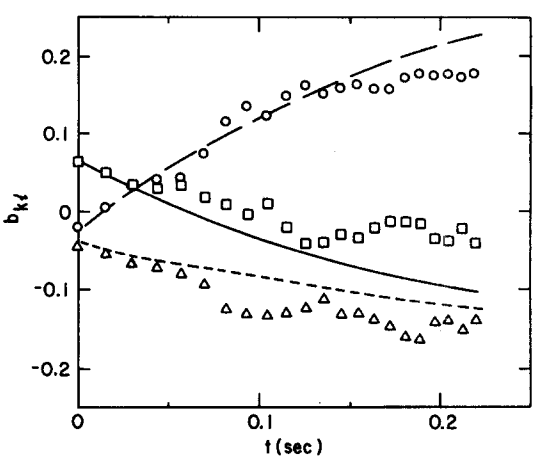

FIG. 20. Evolution of anisotropies b_{kl} for the equivalent symmetric diffuser experiment of Tucker,[42] $D = 7.12$/sec. Lines and symbols are the same as in Fig. 14.

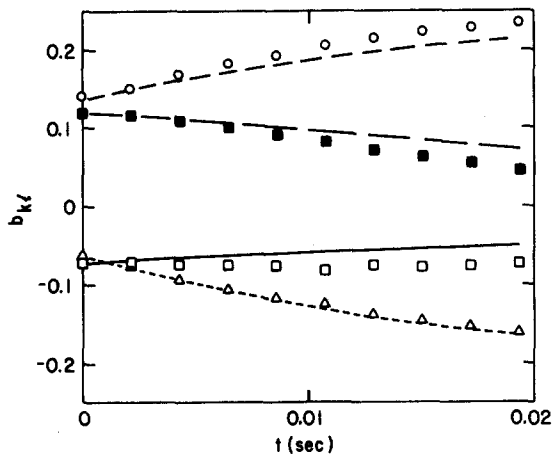

FIG. 21. Evolution of anisotropies b_{kl} for the transverse plane strain experiment of Gence and Mathieu,[44,45] $\alpha = \pi/8$, $D = 32.23$/sec. Langevin model calculations (lines), experimental data (symbols): □, b_{11}; △, b_{22}; ○, b_{33}; ■, b_{23}.

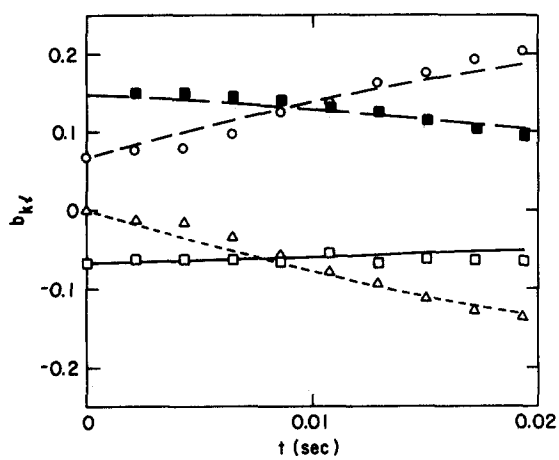

FIG. 22. Evolution of anisotropies b_{kl} for the transverse plane strain experiment of Gence and Mathieu,[44,45] $\alpha = \pi/4$, $D = 32.23$/sec. Lines and symbols are the same as in Fig. 21.

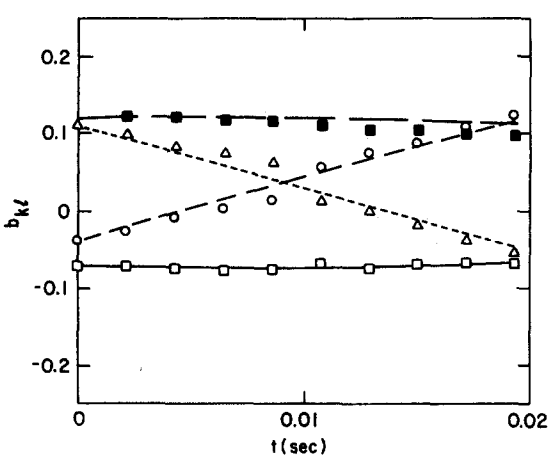

FIG. 23. Evolution of anisotropies b_{kl} for the transverse plane strain experiment of Gence and Mathieu,[44,45] $\alpha = 3\pi/8$, $D = 32.23$/sec. Lines and symbols are the same as in Fig. 21.

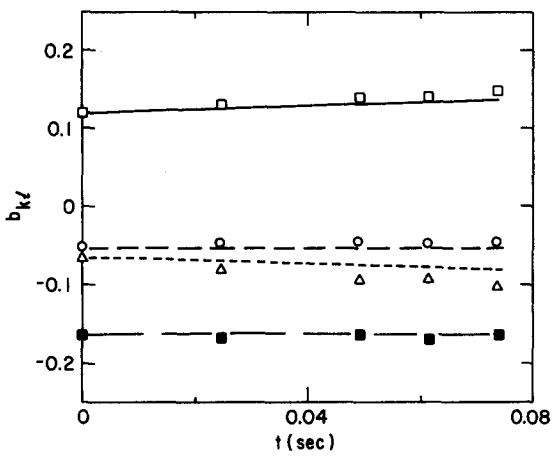

FIG. 24. Evolution of anisotropies b_{kl} for the homogeneous shear flow experiment of Champagne *et al.*,[51] $D = 12.9$/sec. Langevin model calculations (lines), experimental data (symbols): □, b_{11}; △, b_{22}; ○, b_{33}; ■, b_{12}.

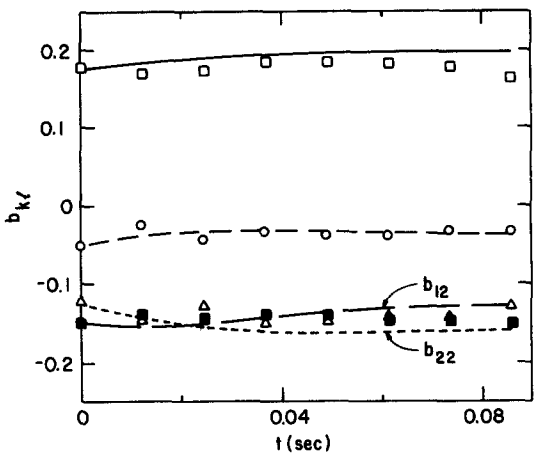

FIG. 25. Evolution of anisotropies b_{kl} for the homogeneous shear flow experiment of Harris *et al.*,[52] $D = 44.0$/sec. Lines and symbols are the same as in Fig. 24.

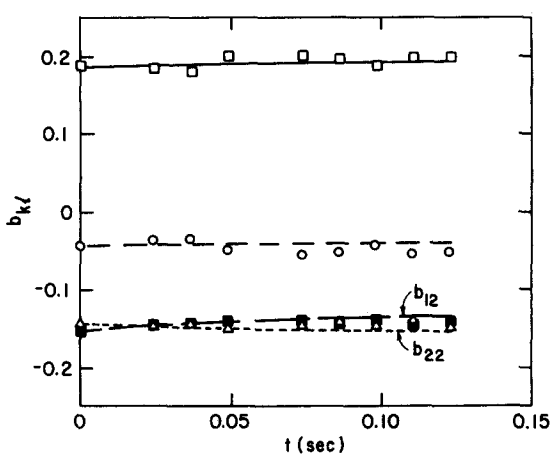

FIG. 26. Evolution of anisotropies b_{kl} for the homogeneous shear flow experiment of Tavoularis and Corrsin,[32] $D = 46.8$/sec. Lines and symbols are the same as in Fig. 24.

Sec. V, $dk/dt = 2kD(b_{33} - b_{11}) - \epsilon$ for this flow. The mean strain rate $D = S_{11}(D > 0)$ is given, $\tau = k/\epsilon$ is taken from the experimental data, and the modeled $b_{33} - b_{11}$ is a bit too large at the downstream end (Fig. 19), hence we might expect the modeled k to grow too quickly there. The difference between model and experiment is less than 10%.

The modeled evolution of b_{kl} is also in reasonable agreement with experimental data in all cases. No systematic departure from experimental behavior is evident in Figs. 14–26, although there are differences in specific cases. The following observations are made:

(i) Agreement is worst in the equivalent symmetric diffuser experiment of Tucker (Fig. 20). The model overpredicts b_{33}, the component in the direction in which the duct expands ($S_{33} = -D < 0$), and underpredicts the streamwise component b_{11}. There is a large scatter in the experimental data for this flow.

(ii) The modeled evolution of b_{11} in the axisymmetric contraction experiment of Tucker deteriorates near the downstream end of the distortion (Fig. 14). Recall from Sec. V that there was some difficulty in extracting ϵ from the experimental data for this flow.

(iii) Agreement is quite good in the flows of type 2 of Sec. V, in which the orientation of the mean strain changes suddenly (Figs. 21–23). There is some tendency for the modeled evolution of b_{23} to lag the experimental data as the principal axes of b_{kl} rotate to align with those of the applied mean strain.

(iv) The model copes equally well with both the weak and the strong homogeneous shear flows (Figs. 24–26). The evolution of b_{12} in the flow of Harris *et al.* Fig. 25 is not as good as in the nearly identical flow of Tavoularis *et al.* (Fig. 26).

We conclude that the optimized model yields quantitative agreement with experimental data in homogeneous flows subject to irrotational mean deformations as well as to both weak and strong mean shear.

It is of interest to examine the sensitivity of these results of changes in the model constants from the optimum values of Eqs. (58) and (59). We denote the optimum model groups of Eq. (58) by $\mathbf{g}^*$, a vector of length 4. By definition, the error $e(\mathbf{g})$ is a minimum for $\mathbf{g} = \mathbf{g}^*$ and hence

$$\left.\frac{\partial e(\mathbf{g})}{\partial g_i}\right|_{\mathbf{g}=\mathbf{g}^*} = 0, \quad i = 1,2,3,4. \tag{60}$$

A sensitivity analysis then requires examination of the second derivatives

$$e_{ij} \equiv \left.\frac{\partial^2 e(\mathbf{g})}{\partial g_i \, \partial g_j}\right|_{\mathbf{g}=\mathbf{g}^*}, \tag{61}$$

where e_{ij} is a symmetric positive semidefinite matrix. This matrix is evaluated numerically by finding $e(\mathbf{g})$ at 32 points in the neighborhood of $\mathbf{g}^*$ and applying the usual finite difference formula for second partial derivatives (see Ref. 53, for example). Next, the eigenvalues and eigenvectors of e_{ij} are found. The eigenvector corresponding to the largest eigenvalue gives the direction in which $e(\mathbf{g})$ increases most rapidly from its minimum at $\mathbf{g} = \mathbf{g}^*$; the eigenvector corresponding to the smallest eigenvalue gives the direction in which $e(\mathbf{g})$ increases least rapidly. Thus the eigenvectors of e_{ij} are the appropriate principal directions in $\mathbf{g}$ space with origin at $\mathbf{g}^*$ in which to examine the sensitivity of the results to changes in the model constants.

The eigenvalues $\lambda^{(i)}$ and eigenvectors $\mathbf{v}^{(i)}$ (normalized to unit Cartesian length) are found to be

$$\begin{aligned}
&\lambda^{(1)} = 3.14, \\
&\mathbf{v}^{(1)} = \{0.135, \ -0.429, \ -0.0877, \ 0.889\}, \\
&\lambda^{(2)} = 0.0222, \\
&\mathbf{v}^{(2)} = \{0.453, \ -0.547, \ -0.586, \ -0.390\}, \\
&\lambda^{(3)} = 0.00413, \\
&\mathbf{v}^{(3)} = \{-0.758, \ -0.620, \ 0.109, \ -0.173\}, \\
&\lambda^{(4)} = 0.00184, \\
&\mathbf{v}^{(4)} = \{-0.451, \ 0.364, \ -0.798, \ 0.165\}.
\end{aligned} \tag{62}$$

The striking finding is that the first eigenvalue is larger than the other three by at least two orders of magnitude. This shows that for the 12 experiments considered, it is the single combination of model constants defined by the first eigenvector that dominates the modeled evolution of the Reynolds stresses in the vicinity of $\mathbf{g} = \mathbf{g}^*$. Unfortunately, it is not possible to quantify a threshold error $e_{\max}$ such that the modeled evolution of the Reynolds stresses is acceptable for $e(\mathbf{g}) < e_{\max}$ and unacceptable for $e(\mathbf{g}) > e_{\max}$. The adequacy or inadequacy of the model results with respect to the experimental data is a subjective judgment. Still, it is useful to estimate (subjectively) the allowable deviation in $\mathbf{g}$ from $\mathbf{g}^*$ along each of the principal directions. To this end, numerical experiments were performed in which $\mathbf{g} = \mathbf{g}^* + \Delta\mathbf{g}$, where $\Delta\mathbf{g}$ is chosen to lie a specified distance along one of the principal axes of e_{ij}. It is found that moving from $\mathbf{g}^*$ in the $\mathbf{v}^{(1)}$ direction by as little as ± 0.05 gives unacceptable evolution of the Reynolds stresses for the two strong shear flows. The allowable deviations in the remaining principal directions are much larger, as expected: ± 0.3 for $\mathbf{v}^{(2)}$, and ± 1.0 for each of $\mathbf{v}^{(3)}$ and $\mathbf{v}^{(4)}$. In all cases it is the modeled evolution of the Reynolds stresses for one of the three shear flows that is most sensitive to changes in the model constants away from the optimum values.

We now turn to the case of decaying turbulence. Several wind tunnel experiments have been performed to study the decay of grid turbulence in the absence of mean velocity gradients. Two principal observations are made in such flows: the turbulent kintic energy k decays and the Reynolds stresses tend toward isotropy ($b_{kl} \to 0$). Recently, efforts have been directed at compiling all available data in these flows, primarily in order to determine the proper modeling of the term $\phi_{ij}^{(2)}$ in second-order closures.[54–56]

With $\partial \langle U_p \rangle / \partial x_q$ identically equal to zero, the modeled Reynolds-stress equation (Eq. 37) involves the single model constant $g_1 = \alpha_2$. The behavior of the model is best understood in terms of the quantities introduced by Choi[54]:

$$ds \equiv \frac{dt}{\tau}, \quad \text{normalized time,} \tag{63}$$

$$\rho \equiv -\frac{d\left[\ln(b_{ii}^2)\right]}{ds}, \quad \text{rate of return-to-isotropy,} \tag{64}$$

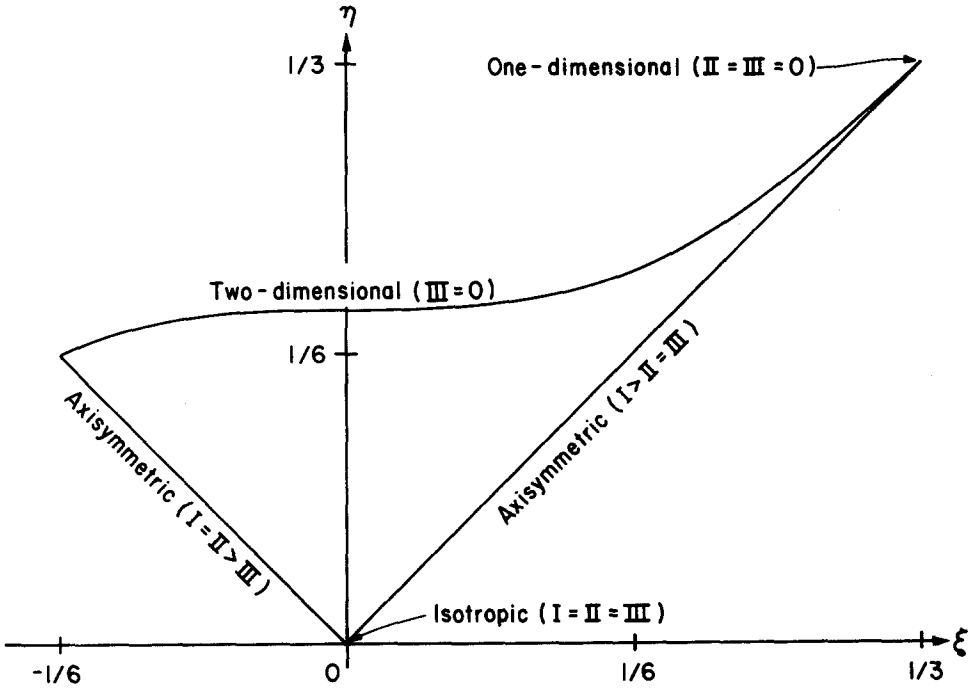

FIG. 27. Allowable region of the ξ-η plane (from Choi[54]); allowable states are confined to the interior of the roughly triangular region. Here I, II, and III denote the eigenvalues of the Reynolds-stress tensor arranged in decreasing order: I>II>III>0.

$$\left.\begin{aligned}\eta &\equiv (1/6b_{ll}^{2})^{1/2},\\ \xi &\equiv (1/6b_{ll}^{3})^{1/3},\end{aligned}\right\} \quad \text{invariants of } b_{kl}. \tag{65}$$

Use of the normalized time ds eliminates the effects of energy decay so that we can concentrate on the return-to-isotropy. The trajectories of the state of the turbulence in the ξ-η plane ($d\eta/d\xi$) and the rate of return-to-isotropy ρ then completely characterize the evolution of the decaying turbulence. A sketch of the allowable region of the ξ-η plane and its physical interpretation is shown in Fig. 27 (see Ref. 54).

The quantities ρ and $d\eta/d\xi$ for the current model are evaluated from Eq. (37). We consider ρ first. All available experimental data lie in the vicinity of the axisymmetric states (Fig. 27). These data indicate that ρ increases with increasing anisotropy (with increasing distance from the origin in Fig. 27) and that for fixed η, ρ is larger for $\xi<0$ than for $\xi>0$. Observed values of ρ vary between 0.0 and approximately 4.0 (for $0.0<\eta<0.13$). The Langevin model, for any α_2 between zero and $2C_0$, gives ρ greater than or equal to zero everywhere in the allowable region of the ξ-η plane. The rate of return-to-isotropy increases with increasing anisotropy except in a narrow regoin near $\xi=\eta$ ($\rho_{\min}$ occurs at $\xi=\eta=\frac{1}{12}$), and for fixed η, ρ is larger for $\xi<0$ than for $\xi>0$. At the extreme states $\xi=\eta=\frac{1}{3}$ and $-\xi=\eta=\frac{1}{6}$, ρ is equal to $3C_0$.

Contours of ρ for $\alpha_2=3.7$ (Eq. 59) are shown in Fig. 28; ρ varies from 0.75 to $3C_0=6.3$ for this α_2. The minimum value, $\rho_{\min}=0.75$, is not as small as the experiments indicate

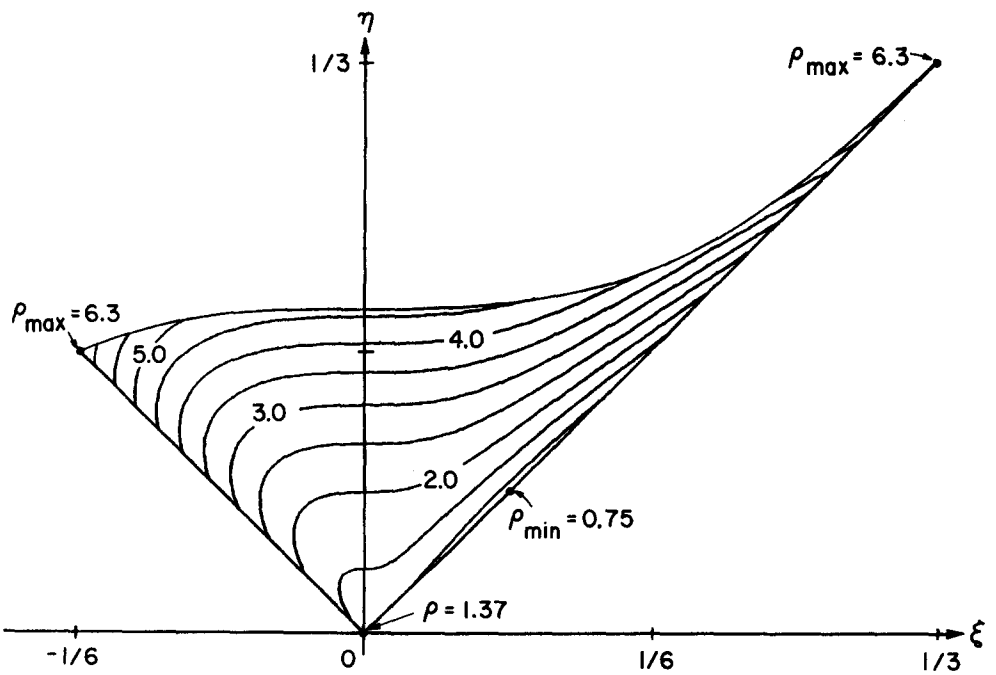

FIG. 28. Contours of constant rate of return-to-isotropy ρ in the ξ-η plane for the Langevin model with $\alpha_2=3.7$.

but $\rho_{\max} = 6.3$ is in somewhat better agreement (recall that measurements are available only up to $\eta \approx 0.13$). The trends noted in the experimental data are evident in Fig. 28. We conclude that the model behaves at least qualitatively correctly in most respects for nearly axisymmetric turbulence.

Experimental data on the trajectories of the return-to-isotropy exhibit the following features: near $\xi = \eta$, the turbulence appears to tend toward the axisymmetric state $\xi = \eta$ as it returns to isotropy; near $\xi = -\eta$, Choi and Lumley[54,55] claim that the turbulence tends toward the axisymmetric state $\xi = -\eta$ as it returns to isotropy, while Le Penven *et al.*[56] claim that it tends away from this state; near $\xi = 0$ (away from the axisymmetric states) there are no data available.

The Langevin model also predicts a tendency toward the axisymmetric state near $\xi = \eta$. Near $\xi = -\eta$ there is a weak tendency toward axisymmetry in a small zone near $\xi = -\eta$; the size of this zone decreases as α_2 increases. Trajectories are horizontal at $\xi = 0$, crossing from negative values of ξ to positive values. In general, there is a sweeping toward the right side of the allowable region of Fig. 27 that increases in intensity as α_2 increases. This behavior is shown in Fig. 29 for $\alpha_2 = 3.7$. Again, we conclude that the model behavior is at least qualitatively correct for this value of α_2.

It is evident that further data are needed on the return-to-isotropy of decaying turbulence, particularly for states far from axisymmetry. We expect that direct numerical simulations and further experimental investigations will resolve this question shortly. That is why we do not select α_2 here by modeling experiments in decaying turbulence. When more complete data are available, we may modify our choice of α_2 or we may even make α_2 a function of ξ and η. We emphasize that the single model constant α_2 yields the complex behavior of Figs. 28 and 29, and that this behavior is in at least qualitative agreement with most aspects of the experimental data in the vicinity of the axisymmetric states.

As a final example of homogeneous flows, we consider the solid body rotation of initially isotropic turbulence. This flow was first studied experimentally by Traugott[57]; Bardina *et al.*[58] performed direct numerical simulations of these and later experiments (see Ref. 58 for references) and provide a physical interpretation of the results. A turbulent Rossby number is defined as $\mathrm{Ro}_T = (\sqrt{2k/3})(1/\Omega\lambda)$, where λ is the Taylor microscale of the turbulence and Ω is the angular velocity of the imposed solid body rotation. The primary results of the experiments and computations can then be expressed in terms of Ro_T: for moderate angular velocities ($\mathrm{Ro}_T > \sim 0.4$) the principal effect of the rotation is to decrease the dissipation rate ϵ with only a small increase in anisotropy of the Reynolds stresses; for extremely high angular velocities ($\mathrm{Ro}_T < \sim 0.2$) the turbulence approaches a two-dimensional state in accord with the Taylor–Proudman theorem.[59] Although this is essentially an inviscid phenomenon, it is the small scales of the turbulence that are most strongly affected by the rotation. The appropriate turbulent time scale is the Kolmogorov microscale $\tau_\eta \approx \lambda/\sqrt{2k/3}$. Thus the alternative expression $\mathrm{Ro}_T = (\tau_\eta \Omega)^{-1}$ shows more clearly why the Rossby number is the appropriate dimensionless parameter.

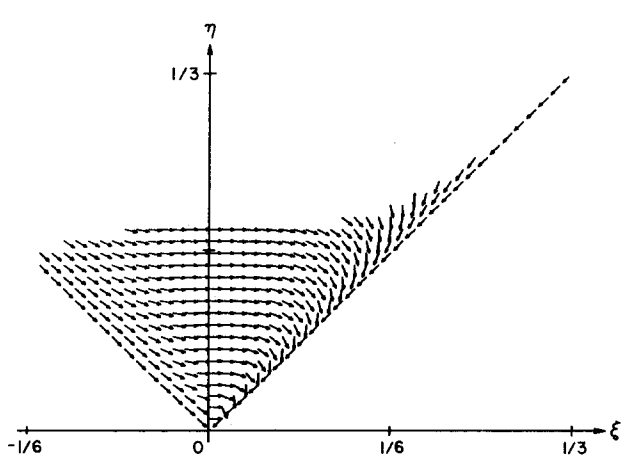

FIG. 29. Trajectories of return-to-isotropy in the ξ-η plane for the Langevin model with $\alpha_2 = 3.7$. Arrows indicate direction only, not rate of return-to-anisotropy.

Consider a solid body rotation about the x_3 axis. Then S_{pq} is identically zero and only $R_{21} = -R_{12} = \Omega$ is nonzero. The x_1 and x_2 directions are indistinguishable; symmetry requires that $\langle u_1 u_2 \rangle = \langle u_1 u_3 \rangle = \langle u_2 u_3 \rangle = 0$ and $\langle u_1^2 \rangle = \langle u_2^2 \rangle$ in the fully developed turbulent flow. The Reynolds-stress evolution equations (Eqs. 18 and 22) reduce to

$$\begin{aligned} \frac{d\langle u_3^2 \rangle}{dt} &= 2\phi_{33} - \epsilon_{33}, \\ \frac{d\langle u_1^2 \rangle}{dt} &= \frac{d\langle u_2^2 \rangle}{dt} = 2\phi_{11} - \epsilon_{11}, \\ \frac{dk}{dt} &= -\epsilon. \end{aligned} \tag{66}$$

This shows that there are no production terms in this flow. The effect of the solid body rotation enters only via its effects on ϕ_{ij}, ϵ_{ij}, and ϵ. Furthermore, $\langle u_3^2 \rangle$ differs from $\langle u_1^2 \rangle = \langle u_2^2 \rangle$ only to the extent that the rotation induces anisotropy in ϕ_{ij} and ϵ_{ij} (assuming isotropy initially). The experimental results stated earlier imply that for moderate rotation rates, little anisotropy is induced in ϕ_{ij} or in ϵ_{ij}.

The Langevin model (Eq. 37) reduces to a set of equations that is identical to the modeled Reynolds-stress equations for decaying turbulence; Ω does not appear. So, the only effect of the solid body rotation on the modeled Reynolds stresses is via its effect on ϵ. We conclude that the Langevin model is consistent with experimental data (to the extent that the anisotropy is negligible) for Ro_T larger than about 0.4. Recall that no ϵ equation is included in the current model.

The Langevin model is incapable of producing a two-dimensional turbulence in the limit $\mathrm{Ro}_T \to 0$. We claim that this limit is outside of the intended range of the model. The mechanism for the approach to the two-dimensional state, according to the Taylor–Proudman theorem, is that Coriolis forces tend to align vortex tubes with the axis of rotation.[58,59] Since vorticity is concentrated in the small scales of the turbulence, local isotropy is destroyed before anisotropy is generated in the Reynolds stresses, a result confirmed in the computations of Bardina *et al.*[58] The vortex stretching

mechanism for the transfer of energy from the large scales of the turbulence to the smaller scales is disrupted, trapping the essentially isotropic energy in the largest scales. Such behavior is clearly beyond the scope of our model. It is in marked contrast to the case of rapid distortion by a mean strain discussed earlier in which production terms are nonzero and the largest scales are deformed most severely by the mean flow.

For the case in which $\langle u_3^2 \rangle \neq \langle u_1^2 \rangle = \langle u_2^2 \rangle$ initially, the model predicts a return-to-isotropy while the data show a decaying state in which $\langle u_3^2 \rangle$ remains greater than $\langle u_1^2 \rangle$. The anisotropy is small for Ro_T greater than 0.4, and to the extent that anisotropy is negligible, the model is again consistent with experimental data.

To summarize, we have presented a set of constants for which the model is in quantitative agreement with available experimental data in homogeneous flows subject to uniform mean deformations. The sensitivity of these results to changes in the model constants was examined. Qualitative agreement with data in decaying grid turbulence and in solid body rotation of nearly isotropic turbulence has also been demonstrated.

VII. CONCLUSION

A generalized Langevin model has been developed by determining the form of the second-order tensor G_{ij} that appears in a general modeled equation for the fluid particle velocity increment. This model provides closure for both the pdf evolution equation and for the Reynolds-stress equations, satisfies realizability, yields joint normal pdf's in homogeneous flows, and is consistent with Kolmogorov's inertial range scaling. We expect the model to describe correctly the behavior of a fluid particle in a turbulent flow only when local isotropy prevails.

The form of the second-order tensor is evaluated by considering the evolution of the Reynolds stresses in homogeneous turbulent flows. We assume a form that is linear in the normalized anisotropy tensor and in the mean velocity gradients. The resulting model cofficients are determined by first comparing the modeled Reynolds-stress evolution equation to its exact counterpart derived from the Navier–Stokes equations. Seven constraints are derived by enforcing proper evolution of the turbulent kinetic energy and by ensuring proper behavior in the limits of a rapid distortion and a two-dimensional turbulence. The four remaining model constants are then found by matching the modeled evolution of the Reynolds stresses to twelve sets of experimental data in homogeneous flows with uniform mean velocity gradients.

An optimum set of coefficients is presented for which the model yields good agreement with experimental data in homogeneous flows subject to mean deformations. In addition, the optimized model exhibits qualitatively correct behavior in decaying turbulence and agrees in a limited sense with experimental data on the solid body rotation of nearly isotropic turbulence for moderate rotation rates.

While the second-order tensor G_{ij} was evaluated by restricting attention to homogeneous turbulent flows, we emphasize that the model is not limited to such flows. The significance of this model lies not in its ability to accurately reproduce the evolution of the Reynolds stresses in homogeneous turbulence (although the level of agreement is encouraging), but rather in the following observations:

(i) both Lagrangian and Eulerian statistics may be extracted from the model[8];

(ii) the extension to multi-time pdf's is straightforward[8]; no additional scale information is then required, and a separate ϵ equation is not needed;

(iii) because Eq. (3) is a closure model for a pdf evolution equation, the extension to the inhomogeneous case requires little further modeling[7]; and

(iv) because G_{ij} also provides closure for second-order models, this pdf method can be used to construct second-order models that satisfy realizability without applying any additional constraints.[33]

The Reynolds-stress model for homogeneous turbulence corresponding to the Langevin model developed here is found from Eqs. (17), (18), and (37), with the optimum model constants given in Eq. (59) and $C_0 = 2.1$:

$$\begin{aligned}\phi_{kl} + \phi_{lk} - \epsilon_{kl} = & -8.3\epsilon b_{kl} - 2/3\epsilon\delta_{kl} + 14.8\epsilon\left[1/3b_{kl} + b_{ki}b_{il} - b_{ii}^2(b_{kl} + 1/3\delta_{kl})\right] \\ & + 1.2k\left[2/3S_{kl} + S_{ki}b_{il} + S_{li}b_{ik} - 2I_1(b_{kl} + 1/3\delta_{kl})\right] + 1.66kb_{is}(S_{sk}b_{il} + S_{sl}b_{ik}) \\ & + 4.8kS_{is}b_{ks}b_{il} + 1.36k\left[b_{ls}S_{sk} + b_{ks}S_{sl} - 2(I_1 + 3I_2)(b_{kl} + 1/3\delta_{kl})\right] \\ & + 0.54k(R_{ki}b_{il} + R_{li}b_{ik}) - 10.38kb_{is}(R_{sk}b_{il} + R_{sl}b_{ik}). \end{aligned} \tag{67}$$

Since homogeneous turbulent flows are ideally suited to direct numerical simulation (see Ref. 60, for example), we expect that G_{ij} could be measured in such simulations. We may find that the linear form assumed here needs to be modified or that the model coefficients must be functions of invariants and of a Reynolds number, at least. Direct simulations should also prove valuable in clearing up lingering uncertainties concerning the return-to-isotropy of decaying turbulence and the proper modeling of $\phi_{ij}^{(2)}$. The optimum set of model constants reported here should not be taken as final until this work has been done. The sensitivity analysis of Sec. VI shows that there is sufficient latitude in the choice of model constants that additional data could be matched without significantly degrading the results for the flows considered here; three degrees of freedom corresponding to the eigenvectors $\mathbf{v}^{(2)}$, $\mathbf{v}^{(3)}$, $\mathbf{v}^{(4)}$ of Eq. (62) remain available. Fu-

ture papers will deal with the application of this Langevin model to inhomogeneous flows and to flows with scalar transport.

ACKNOWLEDGMENT

This work was supported in part by Grant No. CPE-8212661 from the National Science Foundation, Engineering Energetics Program.

[1]B. E. Launder and D. B. Spalding, *Mathematical Models of Turbulence* (Academic, New York, 1972).
[2]B. E. Launder, G. J. Reece, and W. Rodi, J. Fluid Mech. **68**, 537 (1975).
[3]J. L. Lumley, Adv. Appl. Mech. **18**, 123 (1978).
[4]T. S. Lundgren, Phys. Fluids **12**, 485 (1969).
[5]C. Dopazo and E. E. O'Brien, Acta Astronautica **1**, 1239 (1974).
[6]S. B. Pope, Phys. Fluids **24**, 588 (1981).
[7]S. B. Pope, Progress in Energy and Combustion Science **11**, 119 (1985).
[8]S. B. Pope, Phys. Fluids **26**, 404 (1983).
[9]G. I. Taylor, Proc. London Math. Soc., Ser. 2: **20**, 196 (1921).
[10]E. Krasnoff and R. L. Peskin, Geophys. Fluid Dyn. **2**, 123 (1971).
[11]A. M. Yaglom, Fluid Dyn. Trans. **7**, 99 (1976).
[12]P. A. Durbin, NASA Report No. 1103, 1983.
[13]B. L. Sawford, At. Env. **18**, 2405 (1984).
[14]P. M. Chung, AIAA J. **7**, 1982 (1969).
[15]P. M. Chung, Phys. Fluids **13**, 1153 (1970).
[16]P. M. Chung, AIAA Paper No. 70-722, 1970.
[17]P. M. Chung, Phys. Fluids **15**, 1735 (1972).
[18]P. M. Chung, AIAA Paper No. 72-214, 1972.
[19]P. M. Chung, Phys. Fluids **16**, 980 (1973).
[20]R. J. Bywater and P. M. Chung, AIAA Paper No. 73-646, 1973.
[21]R. H. C. Lee, and P. M. Chung, AIAA J. **13**, 1592 (1975).
[22]P. M. Chung, Combust. Sci Tech. **13**, 123 (1976).
[23]R. J. Bywater, AIAA J. **19**, 969 (1981).
[24]R. J. Bywater, AIAA J. **20**, 824 (1982).
[25]V. R. Kuznetsov, and V. A. Frost, Fluid Dyn. (USSR) **8**, 223 (1973) [Izv. Akad. Nauk SSSR Mekh. Zhid k. Gaza **2**, 58 (1973)].
[26]V. A. Frost, Fluid Mech.-Sov. Res. **4**, 124 (1975).
[27]*Noise and Stochastic Processes*, edited by N. Wax (Dover, New York, 1954).
[28]A. S. Monin and A. M. Yaglom, *Statistical Fluid Mechanics*, (MIT, Cambridge, MA, 1975), Vol. 2, p. 359.
[29]A. M. Obukhov, Adv. Geophys. **6**, 113 (1959).
[30]M. S. Anand and S. B. Pope, in *Turbulent Shear Flows 4*, edited by L. J. S. Bradbury, F. Durst, B. E. Launder, F. W. Schmidt, and J. H. Whitelaw (Springer-Verlag, Berlin, 1985), p. 46.
[31]J. L. Lumley, J. Fluid Mech. **41**, 413 (1970).
[32]S. Tavoularis and S. Corrsin, J. Fluid Mech. **104**, 311 (1981).
[33]J. L. Lumley, J. Appl. Mech. **50**, 1097 (1983).
[34]A. A. Townsend, *The Structure of Turbulent Shear Flow* (Cambridge U.P., London, 1976).
[35]H. Tennekes and J. L. Lumley, *A First Course in Turbulence* (MIT, Cambridge, MA, 1972).
[36]P. Y. Chou, Q. Appl. Math. **3**, 38 (1945).
[37]J. C. Rotta, Z. Phys. **129**, 547 (1951).
[38]W. P. Jones and P. Musonge, in *Fourth Symposium on Turbulent Shear Flows*, edited by L. J. S. Bradbury, F. Durst, B. E. Launder, F. W. Schmidt, and J. H. Whitelaw (University of Karlsruhe, Karlsruhe, 1983), p. 17.18); see also P. Musonge, Ph.D. thesis, University of London, 1983.
[39]J. L. Lumley (private communication).
[40]G. K. Batchelor and I. Proudman, Q. J. Mech. Appl. Math **7**, 83 (1954).
[41]A. A. Townsend, Q. J. Mech. Appl. Math. **7**, 104 (1954).
[42]H. J. Tucker, Ph.D. thesis, McGill University, Montreal, 1970.
[43]H. J. Tucker and A. J. Reynolds, J. Fluid Mech. **32**, 657 (1968).
[44]J. N. Gence, Ph.D. thesis, l'Université Claude Bernard, Lyon, 1979.
[45]J. N. Gence and J. Mathieu, J. Fluid Mech. **93**, 501 (1979).
[46]R. R. Mills, and S. Corrsin, NASA Memo No. 5-5-59W, 1959.
[47]C. G. Speziale, Geophys. Astrophys. Fluid Dyn. **23**, 69 (1983).
[48]M. Avriel, *Nonlinear Programming, Analysis and Methods* (Prentice-Hall, Englewood Cliffs, NJ, 1976).
[49]C. de Boor, *A Practical Guide to Splines* (Springer-Verlag, Berlin, 1978).
[50]U. Karnik, M. S. thesis, University of Ottawa, 1983.
[51]F. H. Champagne, V. G. Harris, and S. Corrsin, J. Fluid Mech. **41**, 81 (1970).
[52]V. G. Harris, J. A. H. Graham, and S. Corrsin, J. Fluid Mech. **81**, 657 (1977).
[53]G. D. Smith, *Numerical Solution of Partial Differential Equations: Finite Difference Methods* (Oxford U.P., London, 1978).
[54]K. S. Choi, Ph.D. thesis, Cornell University, Ithaca, 1983.
[55]K. S. Choi, and J. L. Lumley, *Proceedings of the IUTAM Symposium, Kyoto, 1983: Turbulence and Chaotic Phenomena in Fluids*, edited by T. Tatsumi (North-Holland, Amsterdam, 1984), p. 267.
[56]L. Le Penven, J. N. Gence, and G. Comte-Bellot, in *Frontiers in Fluid Mechanics*, edited by S. H. Davis, and J. L. Lumley (Springer-Verlag, Berlin, 1985).
[57]S. C. Traugott, NACA Report No. TN-4135, 1958.
[58]J. Bardina, J. H. Ferzinger, and R. S. Rogallo, J. Fluid Mech. **154**, 321 (1985).
[59]D. J. Tritton, *Physical Fluid Dynamics* (Van Nostrand Reinhold, New York, 1977).
[60]R. S. Rogallo, NASA Report No. TM-81315, 1981.